



# The chronological and geochemical characteristics of Triassic gabbro diorite in the Hongshuihe area of the East Kunlun Orogenic Belt, Northwest China

Xuan Zhou<sup>1</sup> · Qing-feng Ding<sup>1</sup> · Rui-zhe Wu<sup>1</sup> · Yang Gao<sup>1</sup>

Received: 17 January 2022 / Accepted: 9 March 2022 / Published online: 7 April 2022  
© Saudi Society for Geosciences 2022

## Abstract

In order to enrich the overall understanding of mantle-sourced magmatism and magma evolution in the East Kunlun, petrographic, chronological, and geochemical analyses of the Hongshuihe gabbro diorites in the middle section of the East Kunlun were carried out. Two samples from the Hongshuihe gabbro diorites yielded weighted mean zircon U–Pb ages of  $246.3 \pm 1.2$  Ma and  $238.8 \pm 2.5$  Ma, with an average of 242 Ma (Anisian). The Hongshuihe gabbro diorites are characterized by high  $\text{Al}_2\text{O}_3$  (18.24–20.40%), low  $\text{TiO}_2$  (0.77–1.85%), low  $\text{P}_2\text{O}_5$  (0.03–0.26), and low total alkali content (2.85–14.34%) and are rich in sodium and low in potassium, indicating calc-alkaline gabbro diorites. The studied rocks are generally enriched in light rare earth elements (LREEs) and some large ion lithophile elements (LILEs) (such as Rb, Ba, and K), but are depleted in heavy rare earth elements (HREEs) and some high field-strength elements (HFSEs) (such as Ta and Ti), with a slightly high  $(\text{La}/\text{Yb})_N$  of 1.68–7.28. Combined with the geochemical characteristics and mostly positive  $\epsilon_{\text{HF}}(t)$  values (average of 1.2), the source of the Hongshuihe gabbro diorites is considered to be subducted lithospheric mantle-derived magma. The magma has been assimilated and contaminated by the upper crust material during the process of evolution. According to the analysis of the regional tectonic background of the East Kunlun region, the Hongshuihe gabbro diorites were formed under conditions when the Middle Triassic Paleo-Tethys ocean plate subducted northward, similar to the Middle Triassic Hongshuihe quartz diorites and granites. The rocks were produced by the subduction fluid metasomatism of the continental crust due to partial melting of the subduction oceanic crust under conditions of deep burial, high temperature, and high pressure.

**Keywords** Hongshuihe · Eastern Kunlun Orogen · Gabbro diorite · Paleo-Tethys · Zircon U–Pb geochronology

## Introduction

Hongshuihe is located in Dulan County, Qinghai Province, in northwestern China, and its tectonic position belongs to the middle section of the East Kunlun Orogenic Belt, which was considered to be a late Paleozoic orogenic belt in previous studies. Recently, a large number of studies have shown that it is a composite orogenic belt (Ding et al. 2015; Chen et al. 2017). Its tectonic evolution lasted from the Early Paleozoic to the Cenozoic (Jiang et al. 1992; Liu et al. 2005; Mo et al. 2007; Ding

et al. 2014; Chen et al. 2017), and it experienced two different main stages of tectonic evolution in the early Paleozoic and late Paleozoic to the early Mesozoic, and the abundant Early Paleozoic and Late Paleozoic–Early Mesozoic intrusive rocks exposed in the belt are the products of the Proto-Tethys and Paleo-Tethys phases of the East Kunlun Orogenic Belt (Liu et al. 2012). Exploring the petrography, geochronology, and geochemistry of two sets of intrusive rocks from different periods is beneficial for investigations of the specific tectonic evolution process of the Proto-Tethys and Paleo-Tethys phases of the East Kunlun Orogenic Belt. Previous research on magmatic activity in the East Kunlun have mostly considered granitic rocks. Song et al. (2019) found a 244 Ma adakite in Hongshuihe, belonging to the Middle Triassic, which may be related to the subduction of the Paleo-Tethys Ocean plate in the Triassic, indicating that the Paleo-Tethys Ocean was in the subduction stage. In addition to

Responsible Editor: Domenico M. Doronzo

✉ Qing-feng Ding  
dingqf@jlu.edu.cn

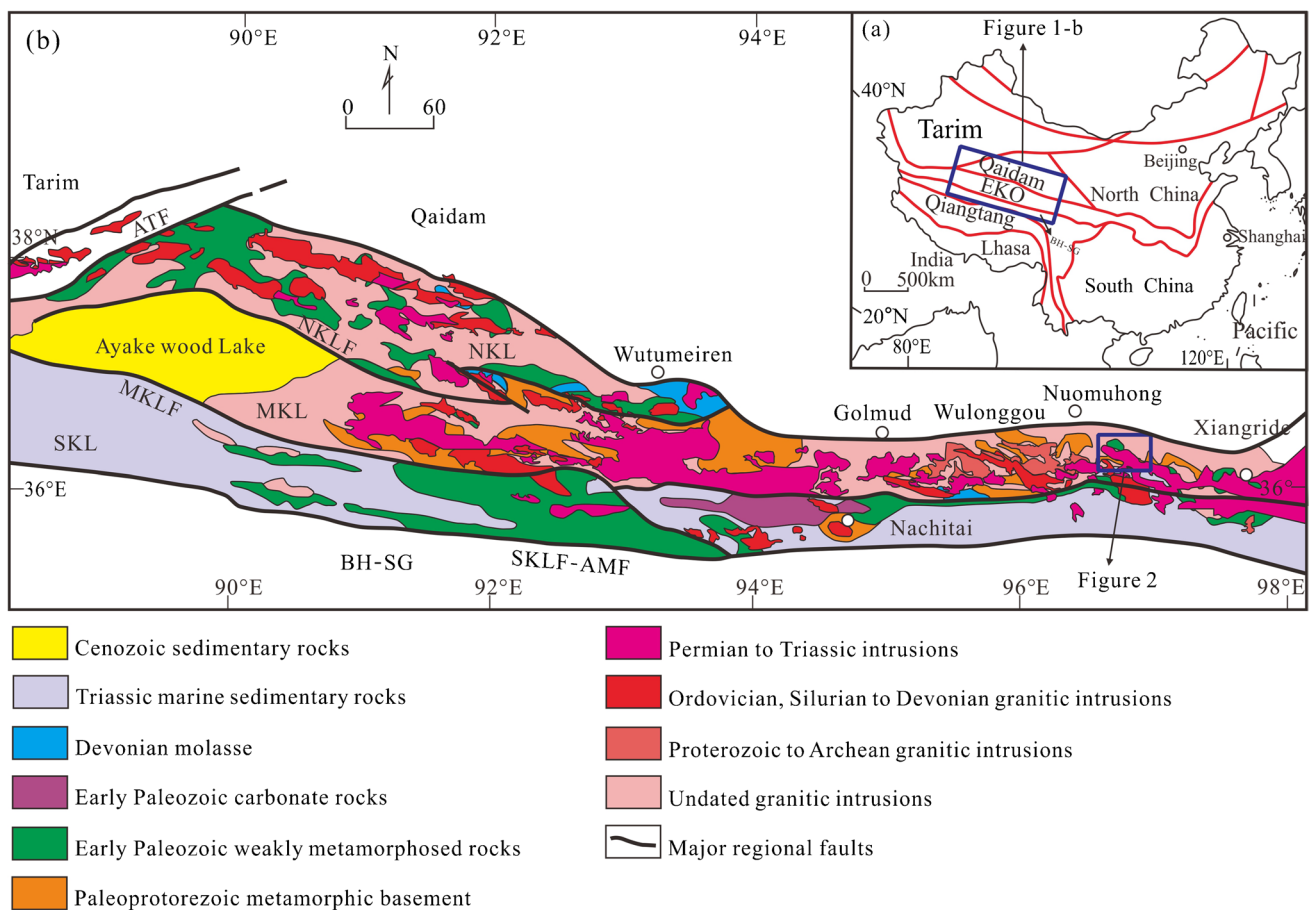
<sup>1</sup> College of Earth Sciences, Jilin University, 2199 Jianshe Street, Changchun 130061, China

the large areas of exposed granites, there are also some intermediate to mafic rocks exposed in the Hongshuihe area. Previous studies on these intermediate mafic rocks are relatively scanty. The intermediate mafic magmatic rocks are used as rock probes for deep sources, although they are less exposed in the East Kunlun Orogenic Belt, but they are of great significance for revealing the nature of the lithospheric mantle and the deep dynamic process, which is helpful for strengthening the overall understanding of the evolution process of magma in the East Kunlun area.

In this study, the petrology, geochronology, and geochemistry of the gabbro diorite pluton exposed in the Hongshuihe area were studied, and the petrogenesis, magma source area, and tectonic significance of the pluton are discussed in order to reveal the nature of the lithospheric mantle and the deep dynamic process, and also to understand the specific tectonic evolution process of the Paleo-Tethys Ocean in the East Kunlun.

## Geological setting

The East Kunlun Orogenic Belt (EKO) is located in the north of the Qinghai–Tibetan Plateau, adjacent to the Qaidam block in the north, connected to the Bayan Har–Songpanganzi accretive complex in the south (Fig. 1). The entire region has experienced four major tectonic evolution stages: Precambrian paleocontinental formation, the Caledonian orogeny, the Late Hercynian–Indosinian orogeny, and the Meso-Cenozoic overlapping orogeny (Liu et al. 2016). The regional tectonic pattern is complex, with three major regional faults running through the area, namely, the North Kunlun Fault (NKLF), the Middle Kunlun Fault (MKLF), and the South Kunlun–Aryan Maqin Fault (SKLF-AMF). According to these faults, Jiang et al. (1992) divided the EKO into three secondary tectonic metallogenic units, namely, the North Kunlun Belt (the Qimantag–Dulan metallogenic belt), the Middle Kunlun belt (the Bokarik–Xiangride metallogenic belt), and the South Kunlun belt (the



**Fig. 1** (a) Sketch tectonic map of China (revised after Yuan et al. 2010). (b) Schematic geological map of the EKO (simplified after Xu et al. 2007). EKO, Eastern Kunlun Orogenic Belt; NKL, North Kunlun Belt; MKL, Middle Kunlun Belt; SKL, South Kunlun Belt;

BH-SG, Bayan Har–Songpanganzi Terrane; ATF, Altyn Tagh Fault; NKLF, North Kunlun Fault (South Qimantag Fault); MKLF, Middle Kunlun Fault; SKLF-AMF, South Kunlun–Aryan Maqin Fault

Xuefengshan–Buerhanbuda metallogenic belt). As a result of regional uplift and three major regional faults, the main structure of the area has a NW–SE trend, in which the NW-trending fault structure is extremely developed, and the regional mineral distribution and the regional stratigraphic distribution are obviously controlled by the fault structure. The East Kunlun Orogenic belt stretches 1200 km along the northern edge of Qinghai and the Qinghai–Tibetan Plateau from west to east (Bian et al. 2004) and provides a wealth of information about the mixed history of the Qinghai–Tibetan Plateau (Ding et al. 2014).

The Hongshuihe area is located in the west of Dulan County, Qinghai Province, and belongs to the Middle Kunlun Belt (Fig. 1b). The exposed strata in the Hongshuihe area include the Paleoproterozoic Jinshuikou Group, the Mesoproterozoic Xiaomiao Formation, the Wanbaogou Formation, the Langyashan Formation, the Carboniferous Halaguole Formation, the Triassic Babaoshan Formation, and the Jurassic Yangqu Formation (Fig. 2).

The rocks of the Paleoproterozoic Jinshuikou Group are distributed across many parts of the area. The strata are mainly distributed in the central and southeastern parts of the area. They are felsic gneiss, including a small amount of marble, plagioclase schist, quartz schist, biotite schist, and muscovite schist, which are the oldest stratigraphic units exposed in the area. The Mesoproterozoic Xiaomiao Formation in the middle and east is composed of limestone, slate, and quartzite, while the Mesoproterozoic Wanbaogou Formation in the west and southeast is composed of dolomite, marble, basalt, and andesite. The central Mesoproterozoic Langyashan Formation is an iron ore-bearing stratum, composed of interbedded limestone, marble, slate, and quartzite. The southern Carboniferous Halagole Formation is composed of andesite, basalt, limestone, and sandstone. The southern Triassic Babaoshan Formation is composed of conglomerate, andesite, tuff, and sandstone. The Jurassic Yangqu Formation mainly occurs between the Mesoproterozoic Langyashan Formation and the Triassic Babaoshan Formation in the middle of Hongshuihe. It is small in scale and is mainly composed of conglomerate, sandstone, and coal interbeds. Some copper polymetallic deposits have been found in the Paleoproterozoic Jinshuikou Group and along the boundary between the Paleoproterozoic Jinshuikou Group and the Mesoproterozoic Langyashan Formation (Song et al. 2019) (Fig. 3).

Affected by the MKLF, which is close to the Hongshuihe area, the tectonic line in the area is SE–NW (Zhang et al. 2009). The area is a wing of the regional folds and is characterized by a stratigraphic monocline (Bao et al. 2010). The faults are widely distributed in Hongshuihe area, mainly divided into nearly E–W trending faults, NE trending faults

that are seriously affected by ore body damage, NNE trending faults, and NW trending faults (Guan 2013; Shen et al. 2009). Moreover, most of the Early–Middle Triassic granitic intrusive bodies have a NW trend. The Hongshuihe gabbro diorite body studied in this article intruded into the Paleoproterozoic Jinshuikou Group strata, as well as Hongshuihe quartz diorite and granite bodies (Song et al. 2019).

## Sample and analytical methods

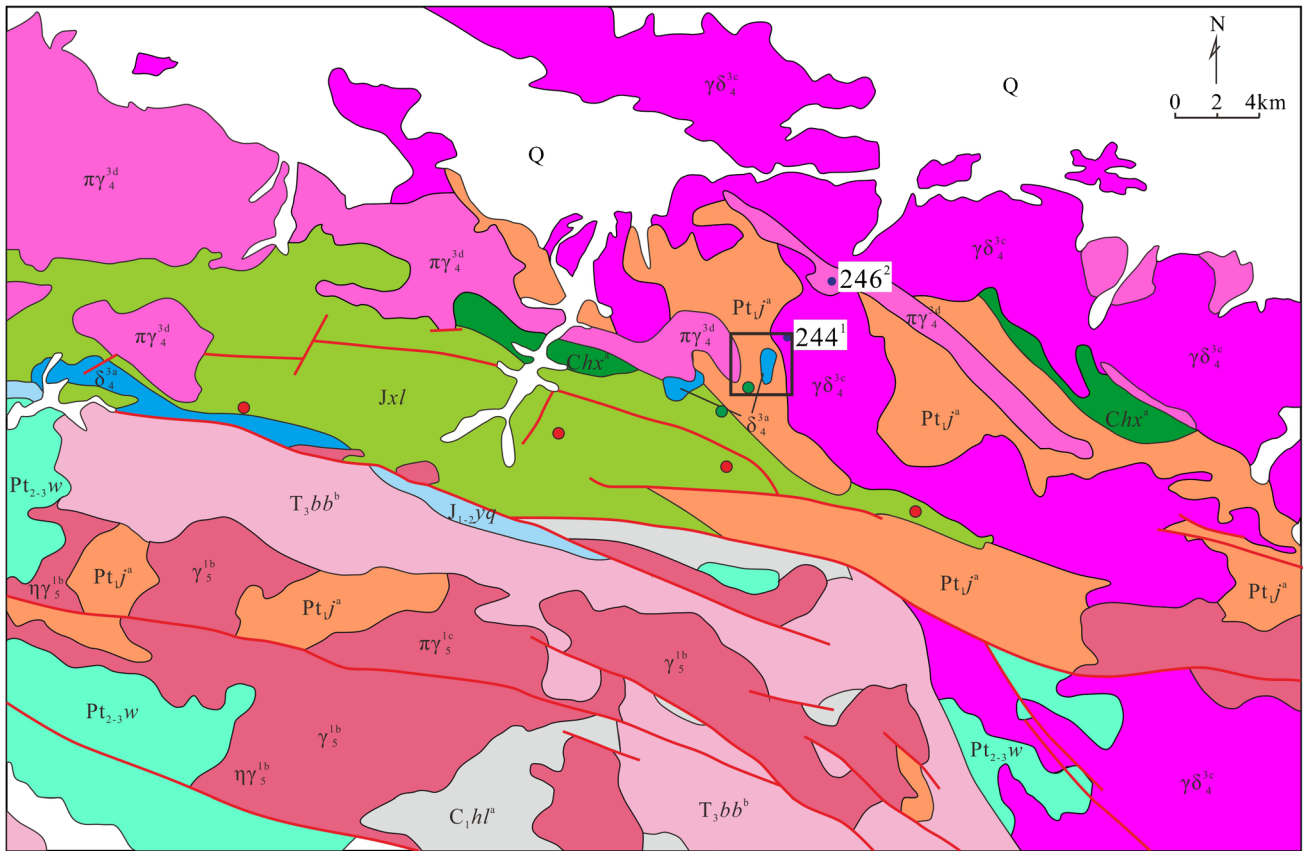
The outcrop of the Hongshuihe gabbro diorite dike intruding into the Paleoproterozoic Jinshuikou Formation is about 1-km long and 400–700-m wide (Fig. 2). It was previously thought to be Hercynian (TIQGS 2014). For this study, seven gabbro diorite samples (HSH03-B1, HSH04-B1, HSH05-B1, 18HSH01-B1, 18HSH02-B1, 18HSH03-B1, and 18HSH04-B1) were collected from surface exposures of the Hongshuihe gabbro diorite dike in Hongshuihe, which are classified as subalkaline. The Hongshuihe gabbro diorite dike consists of plagioclase (40–50%), hornblende (25–45%), pyroxene (2–8%), biotite (5–15%), quartz (about 12%), alkaline feldspar (about 10%), para-minerals magnetite, and sphene (Fig. 4). These rocks have semi-automorphic granular structures and massive structures.

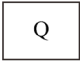
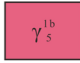
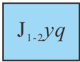

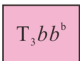
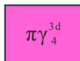
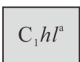
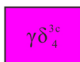
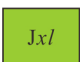

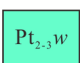



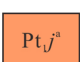
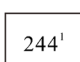
## CL imaging of zircons

Before performing zircon U–Pb dating and Hf isotope analysis, the zircon samples were extracted by crushing, conventional magnetic separation, and gravity separation, and then the zircon particles with high transparency, no inclusions, and no cracks were manually selected. They were then installed in epoxy resin and polished, and the crystals were cut in half for analysis. Finally, zircon U–Pb dating was performed and Hf isotopic CL photos were taken using the cathodoluminescence (CL) detector of a JEOL JSM6510 scanning electron microscope by Beijing Geoanalysis Co., Ltd., to reveal the internal structure of zircon particles.

## LA-ICP-MS zircon U–Pb dating

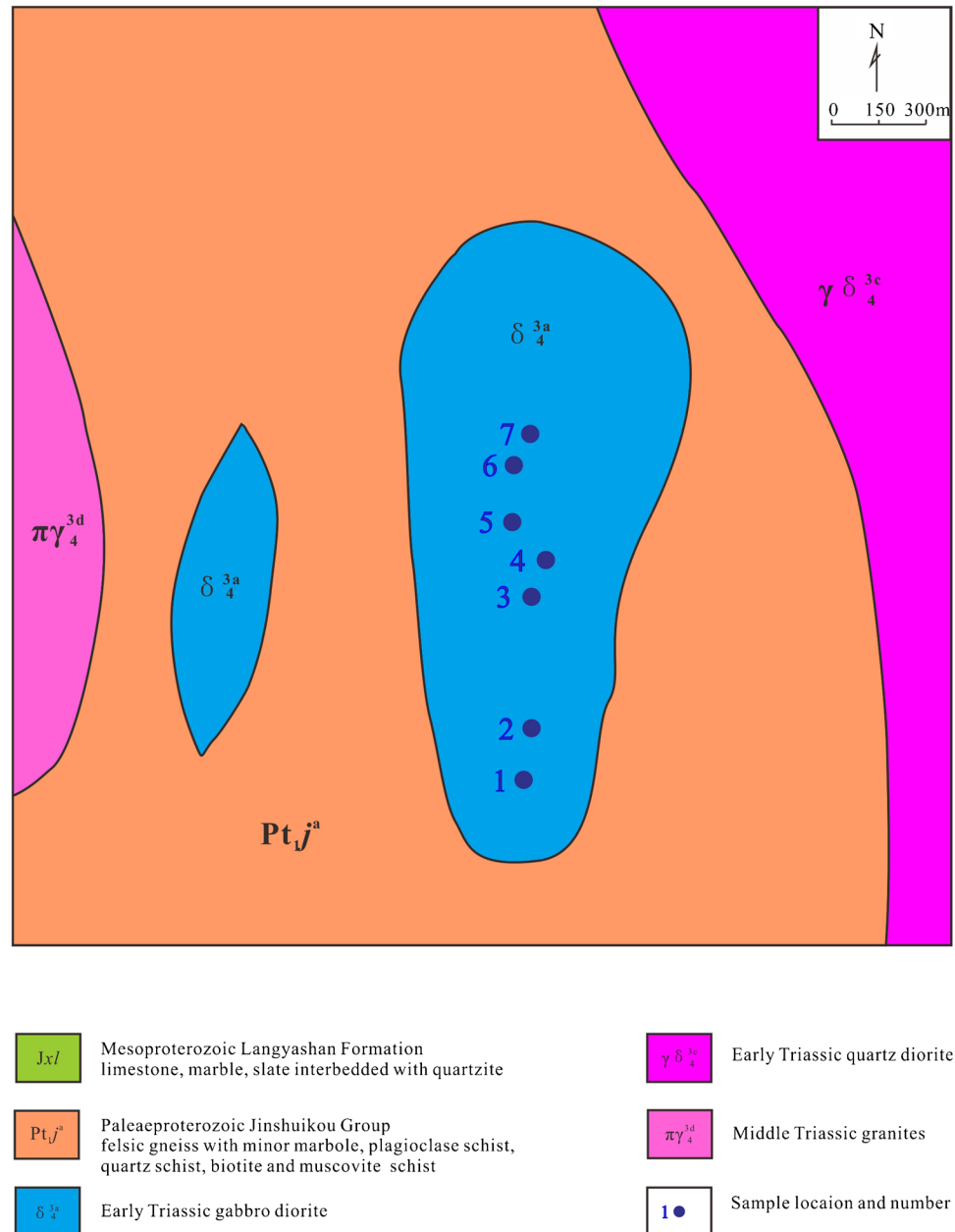
LA-ICP-MS zircon U–Pb dating data of the samples were obtained from Shandong Analysis Center of the Chinese Metallurgical Geology Bureau. The experiment was carried out by a Xseries2 plasma mass spectrometer LA-ICP-MS produced by American Thermoelectric Company with a 193-nm laser ablation system. The detailed operation methods of the laser denudation system and the ICP-MS instrument's parameters are available elsewhere in the literature (Liu et al. 2010). Using 91,500 zircon as the external standards, U–Pb dating was performed for every



	Quaternary alluvial sand and pebble bed		Indosinian granitic rocks
	Jurassic Yangqu Formation conglomerate and sandstone interbedded with coal		Early Triassic gabbro diorites
	Triassic Babaoshan Formation conglomerate, andesite, tuff and sandstone		Early Triassic granites
	Carboniferous Halaguole Formation andesite, basalt, limestone and sandstone		Middle Triassic quartz diorites
	Mesoproterozoic Langyashan Formation limestone, marble, slate interbedded with quartzite		Faults
	Mesoproterozoic Wanbaogou Formation dolomite, marble, basalt and andesite		Fe ore deposits
	Mesoproterozoic Xiaomiao Formation limestone, slate and quartzite		Cu and multimetal ore deposits
	Paleoproterozoic Jinshuigou Group felic gneiss with minor marble, plagioclase schist, quartz schist, biotite and muscovite schist		Age of intrusions

**Fig. 2** Geological map of the Hongshuihe area in the EKO (modified and simplified after TIQGS 2014). Age of intrusions: (1) Hongshuihe quartz diorite, 244 Ma (Song et al. 2019); (2) Hongshuihe granite, 246 Ma (Song et al. 2019)

**Fig. 3** Geologic map of the Hongshuihe gabbro diorites from the Hongshuihe area in the EKO (modified and simplified after TIQGS 2014)



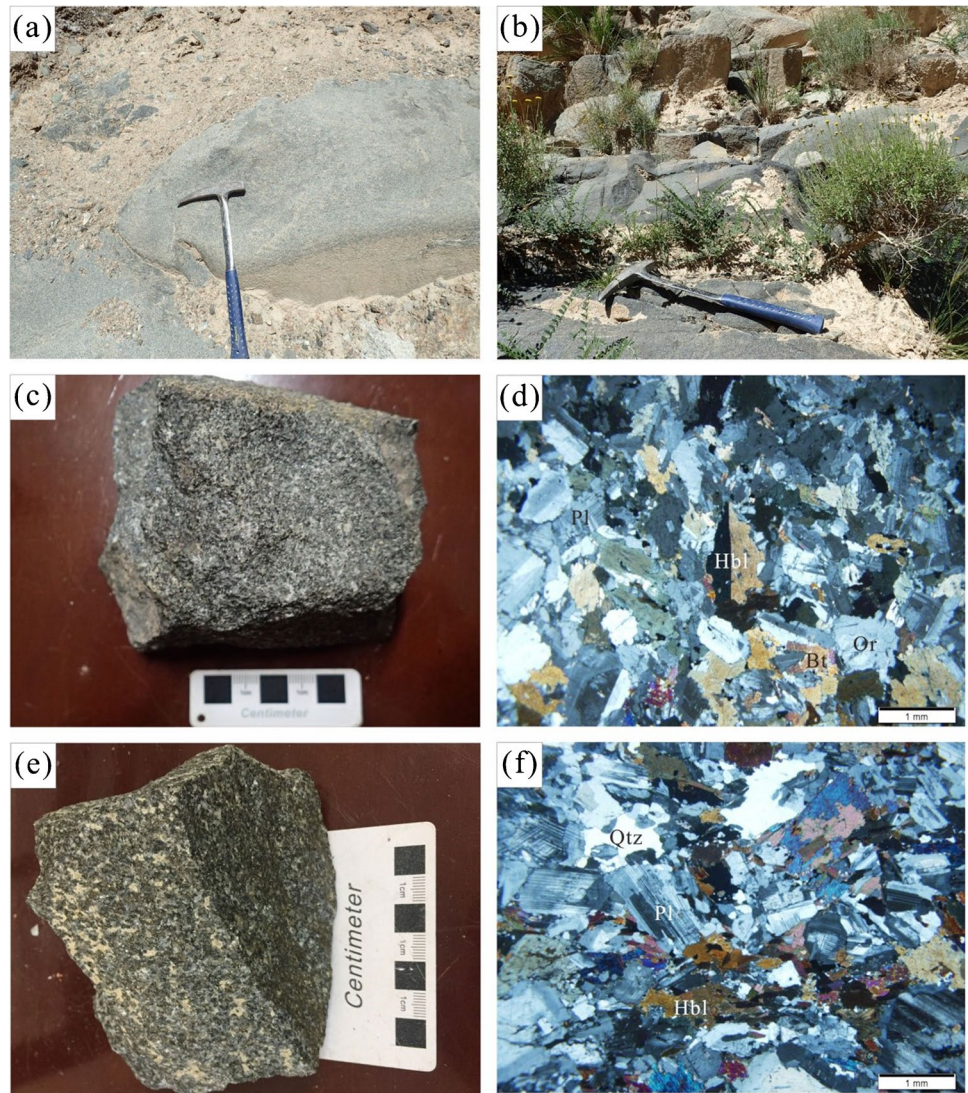
5 zircons, and the drift of the U-Th-Pb isotope ratio over time was corrected twice (Liu et al. 2008, 2010). It can be seen that the background acquisition time of each analysis was 20–30 s, and the data acquisition time was 50 s. ICPMSDataCal was used for offline selection and integration of the background signals and analysis signals, time-shift correction, and quantitative calibration of the U–Pb dating (Liu et al. 2008, 2010).

The commonly used parameter of lead content was assessed using the method described by Andersen (2002). The ages of the harmonic plots were calculated and plotted by using Isoplot V 3.23 (Ludwig 2003).

### Whole-rock major and trace element analyses

All geochemical tests of the samples were performed by the ALS Chemex Co., Ltd. (Guangzhou). Major elements were determined by X-ray fluorescence spectrometry (XRF). Trace elements were determined by inductively coupled plasma–atomic emission spectrometry and inductively coupled plasma–mass spectrometry. The rare earth elements were determined by inductively coupled plasma–mass spectrometry (ICP-MS) with an Agilent7700x spectrometer produced in the USA. In order to facilitate the interpretation of the data, a normalized diagram of spheroidal rare earth

**Fig. 4** Picture of the outcrop of gabbro diorites in the Hongshuihe area. **(a, b)** Representative photographs of the specimens: **(c)** 18HSH03-B1 and **(e)** HSH05-B1, along with micrographs taken under cross-polarized light **(d)** 18HSH03-B1; **(f)** HSH05-B1) of gabbro diorites in the Hongshuihe area. Abbreviations: Bt, biotite; Hbl, hornblende; Pl, plagioclase; Qtz, quartz; Or, orthoclase



elements was also provided. The precision of the major element analysis was better than 5%, and the precision of the trace element and rare earth element analyses was 5–10%. Detailed steps of the operation and the instrument parameter settings are shown elsewhere in the literature (Gou et al. 2013; Ding et al. 2014).

#### LA-MC-ICP-MS zircon Hf isotope analyses

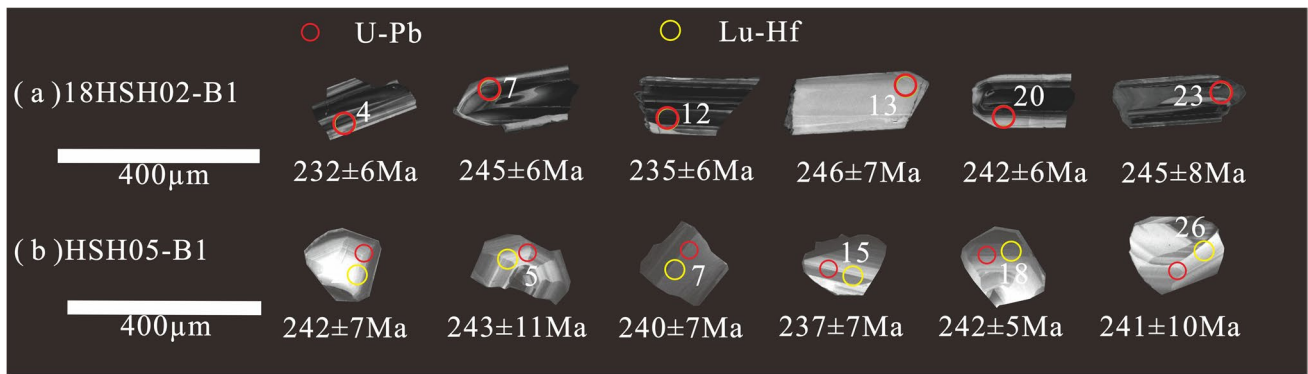
The experiment was conducted using the Neptune II MC-ICP-MS instrument and the New Wave UP213 laser ablation microprobe from the State Key Laboratory for Mineral Deposits Research, Nanjing University. More information on the instrument conditions and data acquisition can be obtained from Wu et al. (2006) and Hou et al. (2007). In the present analysis, a laser 35  $\mu\text{m}$  in diameter was used for in situ analysis. Helium gas was used as the carrier gas, and

a small amount of helium was added into the gas phase carrier, which was beneficial for achieving higher sensitivity.

## Results

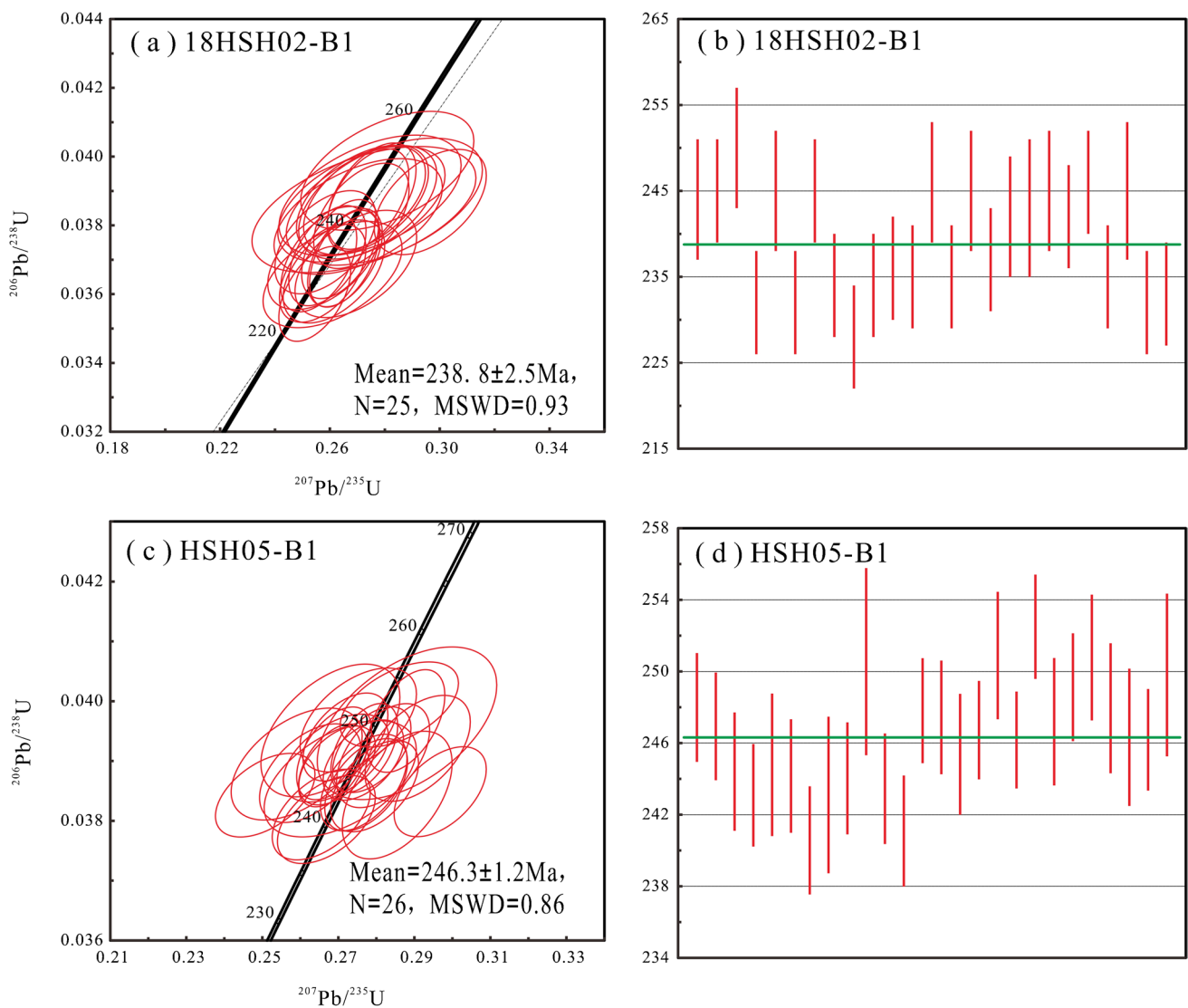
#### Zircon U–Pb ages

The CL images of zircon from the gabbro diorite sample (18HSH02-B1) showed that the zircon grains are dark in color with a long columnar length ratio of 2:1 to 3:1 (250–400  $\mu\text{m}$  in length). The Th/U ratio of the zircon was between 1.38 and 4.07, which further confirmed the magmatic origin. From a total of 25 analysis points, all on the concordia line, the  $^{206}\text{Pb}/^{238}\text{U}$  age was estimated to be 228–250 Ma and the weighted average age was  $238.8 \pm 2.5$  Ma (Fig. 5a, Fig. 6a, b).



**Fig. 5** Representative cathodoluminescence (CL) images of zircons from the Hongshuihe gabbro diorites from the Hongshuihe area in the EKO. (a) Zircon CL images of 18HSH02-B1. (b) Zircon CL images

of HSH05-B1. Red circles in the CL images show the locations of the U–Pb age analyses, and the yellow circles show the locations of the Lu–Hf isotope analyses



**Fig. 6** Zircon U–Pb concordia diagrams for the Hongshuihe gabbro diorites from the Hongshuihe area in the EKO. (a, b) Diagram of zircon U–Pb dating of the HSH02-B1 sample from the Hongshuihe gab-

bro diorites. (c, d) Diagram of zircon U–Pb dating of the HSH05-B1 sample from the Hongshuihe gabbro diorites

Most of the zircons from the gabbro diorite sample (18HSH05-B1) are colorless and mostly granular, with crystal lengths ranging from 100 to 200  $\mu\text{m}$ . Some zircons have obvious zonal structures. Dating analysis of 26 zircons was carried out, and the results are shown in Table 1. The Th/U values of the zircons ranged from 0.36 to 0.92, consistent with magmatic zircons (Th/U > 0.1). All the analyzed data points were located on and near the concordia line. The age of  $^{206}\text{Pb}/^{238}\text{U}$  ranged from  $241 \pm 3$  to  $251 \pm 4$  Ma, and the weighted average age was  $246.3 \pm 1.2$  Ma (MSWD = 0.86) (Fig. 5b, Fig. 6c, d).

In conclusion, the Hongshuihe gabbro diorite samples were formed in the Middle Triassic.

## Major elements

The contents of  $\text{SiO}_2$  in the samples ranged from 46.52 to 54.01%, the total alkali content ( $\text{K}_2\text{O} + \text{Na}_2\text{O}$ ) ranged from 2.85 to 14.34%, and  $\text{Al}_2\text{O}_3$  (18.24 to 20.04%) and  $^{\text{T}}\text{Fe}_2\text{O}_3$  (8.39 to 13.66%) were relatively high. The MgO content was 3.18–5.85%, the CaO content was 7.58–10.45%, the  $\text{Mg}^{\#}$  value ( $\text{Mg}^{\#} = \text{Mg}/(\text{Mg} + \text{Fe}_{\text{T}})$ ) was low (0.40–0.56), and the  $\text{TiO}_2$  content was 0.77–1.85%. The over-alkali index (the  $w(\text{K}_2\text{O} + \text{Na}_2\text{O})/w(\text{Al}_2\text{O}_3)$  molecular ratio) was 0.26–0.35, and the A/CNK aluminum index was 0.79–0.96. In the discriminant diagram of the aluminum index (Fig. 8), all samples fell within the quasi-aluminum region. In the TAS diagram (Fig. 7), the samples were distributed in the subalkaline gabbro and gabbro diorite regions. The  $\text{Na}_2\text{O}/\text{K}_2\text{O}$  of the samples ranged from 2.32 to 8.46. In the diagram of  $\text{K}_2\text{O}$  and  $\text{SiO}_2$  (Fig. 8), the samples are mainly distributed in the calc-alkaline series.

In the Harker diagrams, which display binary major elements vs. MgO variations (Fig. 9), the major elements of the samples of the Hongshuihe gabbro diorites showed no obvious correlations with MgO.

## Trace elements

The total amount of rare earth elements ( $\sum\text{REE}$ ) of the samples from the investigated area was between  $56.45 \times 10^{-6}$  and  $129.32 \times 10^{-6}$ , the content of light rare earth elements (LREEs) was between  $43.67 \times 10^{-6}$  and  $98.15 \times 10^{-6}$ , and the content of heavy rare earth elements (HREEs) was between  $7.33 \times 10^{-6}$  and  $32.61 \times 10^{-6}$ .  $\text{LREE}/\text{HREE} = 2.63\text{--}7.55$  indicates obvious fractionation of LREEs and relatively weak fractionation of HREEs. According to the chondrite normalized distribution diagram (Fig. 10a), the chondrite showed a slight right-leaning distribution pattern of LREE enrichment and a relative deficit of HREE, with  $(\text{La}/\text{Yb})_{\text{N}} = 1.68\text{--}7.28$ . The Europium basically showed no anomaly ( $\delta\text{Eu} = 0.77\text{--}2.35$ ). In the normalized spiderweb map of the original mantle of trace elements (Fig. 10b), the samples

are enriched in large ion lithophile elements (LILEs) such as Rb, Ba, and K, and depleted in high field strength elements (HFSEs) such as Ta and Ti to varying degrees (Table 2).

## Zircon Hf isotopes

In situ zircon Hf isotope analysis of the sample HSH05-B1 was conducted. The specific analysis results are shown in Table 3, and the Hf isotope characteristics of zircon are shown in Fig. 11. The zircon  $^{176}\text{Hf}/^{177}\text{Hf}$  ratios of the diorite (HSH05-B1) ranged from 0.282610 to 0.282685, and the  $\varepsilon_{\text{Hf}}(t)$  values ranged from  $-0.5$  to 3.6, with an average of 1.27. The samples are mainly concentrated near the chondrite line in the partial enlarged diagram of Fig. 11a.

## Discussion

### Geochronology of the Middle Triassic gabbro diorites

This study obtained reliable LA-ICP-MS U–Pb zircon ages from the gabbro diorites intruding into the Mesoproterozoic Jinshuikou Group in the Hongshuihe area of the EKO. Two samples of the Hongshuihe gabbro diorites yielded weighted mean zircon ages of  $238.8 \pm 2.5$  Ma and  $246.3 \pm 1.2$  Ma, with an average age of 242 Ma (Anisian), indicating that the Hongshuihe gabbro diorites were formed in the Middle Triassic. Previous research indicated that the EKO has experienced subduction, syncollision, and post-collision stages (Chen et al. 2017; Ding et al. 2014, 2015; Song et al. 2019). In comparison with the  $244 \pm 2$  Ma (Anisian) Hongshuihe quartz diorites and the  $246 \pm 1$  Ma (Olenekian) granites (Song et al. 2019), the Balugou 244 Ma (Anisian) granites (Ding et al. 2014), the Wulonggou 248 Ma (Olenekian) granodiorites, and the Xiaoyakou  $246 \pm 3$  Ma (Olenekian) granites (Ding et al. 2015), the Hongshuihe gabbro diorites were formed at a similar but slightly later time to these nearby rock dikes, which suggests that the gabbro diorites may be closely related to these rocks, especially the Hongshuihe quartz diorites and granites. Further study on the genesis of the Hongshuihe gabbro diorite will help to limit the subduction time of the Paleo-Tethys Ocean and complete the picture of the tectonic evolution of the East Kunlun orogenic belt.

### Petrogenesis of the Hongshuihe gabbro diorites

#### Petrogenetic type

The TAS diagram showed that the Hongshuihe gabbro diorite samples were distributed across the subalkaline gabbro



**Table 1** LA-ICP-MS zircon U–Pb data for the Hongshuihe gabbro diorites from the Hongshuihe area in the EKO

Sample	<sup>232</sup> Th		Th/U	Isotopic ratios				Isotopic ages (Ma)							
	<sup>238</sup> U	(ppm)		<sup>207</sup> Pb/ <sup>206</sup> Pb	1σ	<sup>207</sup> Pb/ <sup>235</sup> U	1σ	<sup>206</sup> Pb/ <sup>238</sup> U	1σ	<sup>207</sup> Pb/ <sup>235</sup> U	1σ	<sup>206</sup> Pb/ <sup>238</sup> U	1σ		
	(ppm)	(ppm)													
18HSH02-B1															
18HSH02-B1-01	32.4	115.7	3.57	0.05099	0.00377	0.2715	0.02009	0.03862	0.00111	240	117	244	16	244	7
18HSH02-B1-02	175.5	361.7	2.06	0.05127	0.00171	0.27384	0.00983	0.03874	0.00098	253	40	246	8	245	6
18HSH02-B1-03	27.9	81.9	2.93	0.05146	0.00381	0.28091	0.0208	0.03959	0.00114	261	117	251	16	250	7
18HSH02-B1-04	71.1	192.4	2.71	0.05174	0.0033	0.26095	0.0167	0.03657	0.00102	274	96	235	13	232	6
18HSH02-B1-05	65.4	130.9	2.00	0.0508	0.00287	0.27134	0.01552	0.03873	0.00105	232	82	244	12	245	7
18HSH02-B1-06	170.2	378.3	2.22	0.05097	0.00196	0.25736	0.01041	0.03661	0.00094	239	49	233	8	232	6
18HSH02-B1-07	86.9	207.2	2.38	0.05561	0.00244	0.29657	0.01348	0.03868	0.00101	437	56	264	11	245	6
18HSH02-B1-08	336.3	540.9	1.61	0.05028	0.00167	0.25595	0.00914	0.03691	0.00094	208	40	231	7	234	6
18HSH02-B1-09	225.3	500.6	2.22	0.05125	0.00159	0.25449	0.00864	0.03601	0.00091	252	37	230	7	228	6
18HSH02-B1-10	504.0	695.1	1.38	0.05195	0.00147	0.26527	0.00835	0.03703	0.00093	283	33	239	7	234	6
18HSH02-B1-11	85.7	536.2	6.26	0.05125	0.00166	0.26373	0.00927	0.03731	0.00095	252	39	238	7	236	6
18HSH02-B1-12	319.1	536.3	1.68	0.05195	0.0016	0.26549	0.00898	0.03706	0.00094	283	36	239	7	235	6
18HSH02-B1-13	30.0	84.6	2.82	0.05124	0.00409	0.27464	0.02188	0.03887	0.00116	252	127	246	17	246	7
18HSH02-B1-14	45.8	119.0	2.60	0.05046	0.00257	0.25779	0.01347	0.03705	0.00099	216	72	233	11	235	6
18HSH02-B1-15	56.6	145.6	2.57	0.05113	0.00276	0.27317	0.01501	0.03874	0.00105	247	77	245	12	245	7
18HSH02-B1-16	57.4	233.3	4.07	0.04995	0.00226	0.25833	0.01213	0.03751	0.00099	193	62	233	10	237	6
18HSH02-B1-17	24.6	93.1	3.78	0.05124	0.00382	0.27031	0.02024	0.03826	0.00111	252	118	243	16	242	7
18HSH02-B1-18	11.8	46.5	3.94	0.05137	0.0051	0.2724	0.02692	0.03846	0.00121	257	165	245	21	243	8
18HSH02-B1-19	83.5	177.5	2.13	0.05134	0.00308	0.27377	0.0166	0.03867	0.00109	256	88	246	13	245	7
18HSH02-B1-20	185.4	340.1	1.83	0.05144	0.00206	0.27148	0.01147	0.03828	0.00101	261	51	244	9	242	6
18HSH02-B1-21	188.9	357.1	1.89	0.05139	0.00186	0.27525	0.01065	0.03885	0.00102	258	44	247	8	246	6
18HSH02-B1-22	167.4	387.7	2.32	0.05063	0.00167	0.25909	0.00929	0.03712	0.00096	224	40	234	7	235	6
18HSH02-B1-23	135.9	321.6	2.37	0.05246	0.00444	0.27984	0.02357	0.03869	0.00122	306	134	251	19	245	8
18HSH02-B1-24	304.4	592.5	1.95	0.05173	0.00233	0.26145	0.01221	0.03666	0.00099	273	59	236	10	232	6
18HSH02-B1-25	480.1	724.1	1.51	0.05299	0.00281	0.26944	0.01461	0.03688	0.00103	328	73	242	12	233	6
HSH05-B1															
HSH05-B1-01	428.6	641.1	0.67	0.0511	0.0010	0.2768	0.0058	0.0392	0.0005	243	44	248	5	248	3
HSH05-B1-02	64.8	171.4	0.38	0.0502	0.0017	0.2694	0.0091	0.0390	0.0005	206	80	242	7	247	3
HSH05-B1-03	72.8	184.7	0.39	0.0524	0.0015	0.2767	0.0075	0.0386	0.0005	302	67	248	6	244	3
HSH05-B1-04	81.3	200.4	0.41	0.0473	0.0017	0.2508	0.0087	0.0384	0.0005	65	81	227	7	243	3
HSH05-B1-05	68.4	120.7	0.57	0.0505	0.0025	0.2705	0.0132	0.0387	0.0006	220	113	243	11	245	4
HSH05-B1-06	215.3	431.8	0.50	0.0518	0.0013	0.2773	0.0072	0.0386	0.0005	276	57	249	6	244	3
HSH05-B1-07	222.1	336.9	0.66	0.0508	0.0017	0.2668	0.0085	0.0380	0.0005	232	80	240	7	241	3
HSH05-B1-08	124.3	273.9	0.45	0.0537	0.0018	0.2855	0.0095	0.0384	0.0007	367	76	255	8	243	4

**Table 1** (continued)

Sample	<sup>232</sup> Th (ppm)	<sup>238</sup> U (ppm)	Th/U	Isotopic ratios				Isotopic ages (Ma)							
				<sup>207</sup> Pb/ <sup>206</sup> Pb	1σ	<sup>207</sup> Pb/ <sup>235</sup> U	1σ	<sup>206</sup> Pb/ <sup>238</sup> U	1σ	<sup>207</sup> Pb/ <sup>235</sup> U	1σ	<sup>206</sup> Pb/ <sup>238</sup> U	1σ		
HSH05-B1-09	122.9	280.7	0.44	0.0525	0.0015	0.2795	0.0076	0.0386	0.0005	306	67	250	6	244	3
HSH05-B1-10	27.9	77.5	0.36	0.0540	0.0030	0.2881	0.0156	0.0396	0.0008	372	129	257	12	251	5
HSH05-B1-11	587.9	640.8	0.92	0.0557	0.0015	0.2968	0.0080	0.0385	0.0005	439	61	264	6	243	3
HSH05-B1-12	72.1	177.2	0.41	0.0508	0.0017	0.2655	0.0085	0.0381	0.0005	232	78	239	7	241	3
HSH05-B1-13	144.5	333.6	0.43	0.0514	0.0012	0.2788	0.0068	0.0392	0.0005	257	56	250	5	248	3
HSH05-B1-14	169.3	364.6	0.46	0.0503	0.0013	0.2689	0.0065	0.0391	0.0005	209	94	242	5	247	3
HSH05-B1-15	106.3	173.2	0.61	0.0495	0.0017	0.2626	0.0088	0.0388	0.0005	172	75	237	7	245	3
HSH05-B1-16	123.2	316.7	0.39	0.0515	0.0013	0.2766	0.0070	0.0390	0.0004	261	55	248	6	247	3
HSH05-B1-17	69.9	145.5	0.48	0.0507	0.0018	0.2752	0.0101	0.0397	0.0006	233	83	247	8	251	4
HSH05-B1-18	234.6	422.0	0.56	0.0504	0.0012	0.2697	0.0066	0.0389	0.0004	213	90	242	5	246	3
HSH05-B1-19	102.7	257.9	0.40	0.0520	0.0017	0.2860	0.0103	0.0399	0.0005	287	76	255	8	252	3
HSH05-B1-20	215.1	395.8	0.54	0.0522	0.0013	0.2817	0.0081	0.0391	0.0006	295	57	252	6	247	4
HSH05-B1-21	196.1	319.4	0.61	0.0500	0.0013	0.2719	0.0074	0.0394	0.0005	195	27	244	6	249	3
HSH05-B1-22	174.9	443.8	0.39	0.0529	0.0012	0.2878	0.0067	0.0397	0.0006	324	21	257	5	251	4
HSH05-B1-23	88.2	236.4	0.37	0.0545	0.0018	0.2908	0.0091	0.0392	0.0006	391	74	259	7	248	4
HSH05-B1-24	52.2	129.4	0.40	0.0492	0.0023	0.2590	0.0114	0.0389	0.0006	167	111	234	9	246	4
HSH05-B1-25	355.2	553.3	0.64	0.0498	0.0010	0.2685	0.0060	0.0389	0.0005	183	14	241	5	246	3
HSH05-B1-26	35.6	93.1	0.38	0.0501	0.0025	0.2679	0.0121	0.0395	0.0007	211	119	241	10	250	5

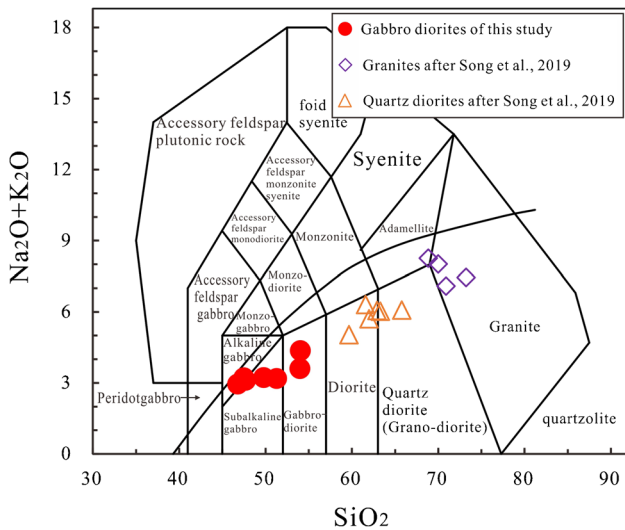


Fig. 7 TAS diagram (modified after Cox et al. 1979)

and gabbro diorite regions. In the discriminant diagram of the aluminum index and the diagram of  $K_2O$  and  $SiO_2$ , they mainly fell within the quasi-aluminum region and the calc-alkaline series, respectively. Compared with subalkaline gabbro, observation of the sample under the microscope showed that the content of pyroxene was only 2–8%, so the possibility of subalkaline gabbro was excluded and the rocks were determined to be gabbro diorite. Furthermore, the  $SiO_2$  content of the gabbro diorites samples was 46.52 ~ 54.01%, with an average of 49.89%, which is higher than that of typical gabbro samples (47.62%) (Zhang 2017). The  $Na_2O$  content was 2.41 ~ 3.89%, the  $K_2O$  content was 0.44 ~ 1.08%, and their mean values were, respectively, 2.74% and 0.62%.

The  $Na_2O$  content was greater than the  $K_2O$  and  $Al_2O_3$  content which was 18.24 ~ 20.40%; the mean value was 19%, which was higher than normal gabbro value, which is 14.52%. The  $CaO$  content was 7.58 ~ 10.45%, showing characteristics of rich sodium, low potassium, rich calcium, and high aluminum, similar to the rocks in typical subduction zones (Zhang and Zhou 2001).

In the chondrite-normalized REE patterns, the light rare earth elements were enriched but the heavy rare earth elements were depleted, and the line of the heavy rare earth elements was nearly flat, probably related to the residue of hornblende. Eu anomalies are often associated with the crystallization process of plagioclase, negative anomalies with the separated crystallization of plagioclase, and positive anomalies with the stacking crystals of plagioclase. The  $\delta Eu$  of the rock samples ranged from 0.77 to 2.35, showing a weak positive Eu anomaly, and there was no correlation between  $Al_2O_3$ ,  $P_2O_5$ , and  $MgO$  in the Harker diagram (Fig. 9), indicating that the separation and crystallization process of plagioclase and apatite was not obvious. The total amount of rare earth elements ( $\sum REE$ ) of the samples was between  $56.45 \times 10^{-6}$  and  $129.32 \times 10^{-6}$ , with an average value of  $93.36 \times 10^{-6}$ , which is higher than that of the original mantle ( $\sum REE = 7.43 \times 10^{-6}$ ), lower than that of the OIB ( $\sum REE = 198.96 \times 10^{-6}$ ), and slightly higher than that of the E-MORB ( $\sum REE = 49.09 \times 10^{-6}$ ) (Sun and McDonough 1989). The distribution curve of rare earth elements is similar to that of the E-MORB, but is obviously different from that of the N-MORB (Fig. 10a), suggesting that the magma came from the enriched mantle source area, but the degree of differentiation of light and heavy rare earth elements is stronger than that of the E-MORB. Furthermore, compared with Hongshuihe granites and quartz diorites, the

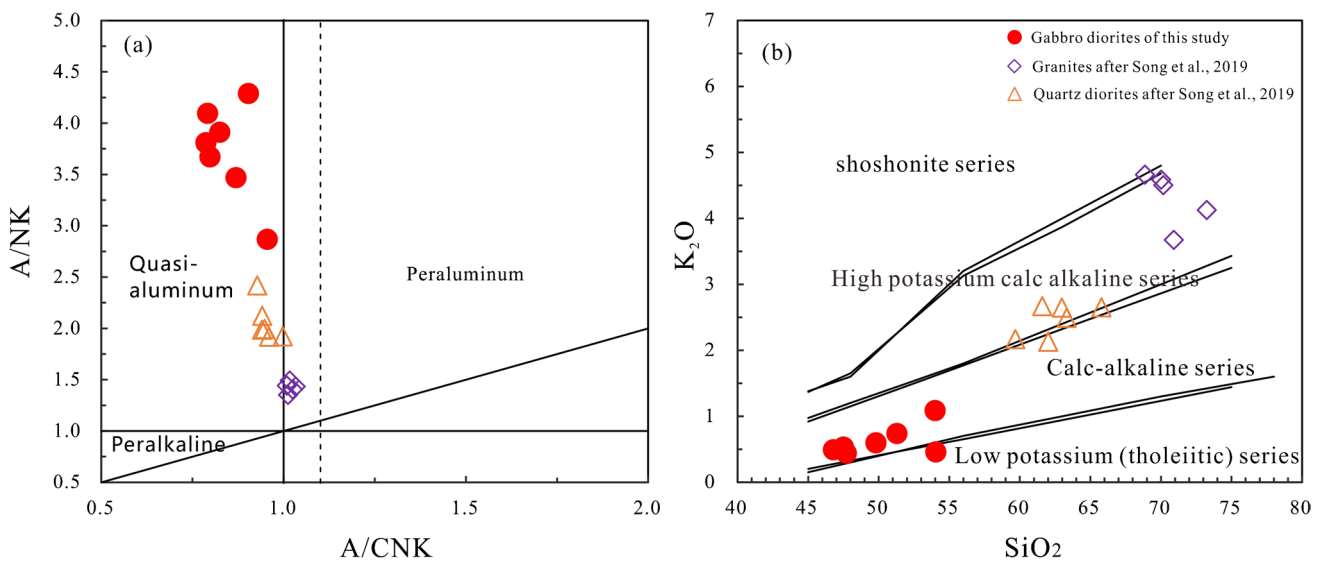
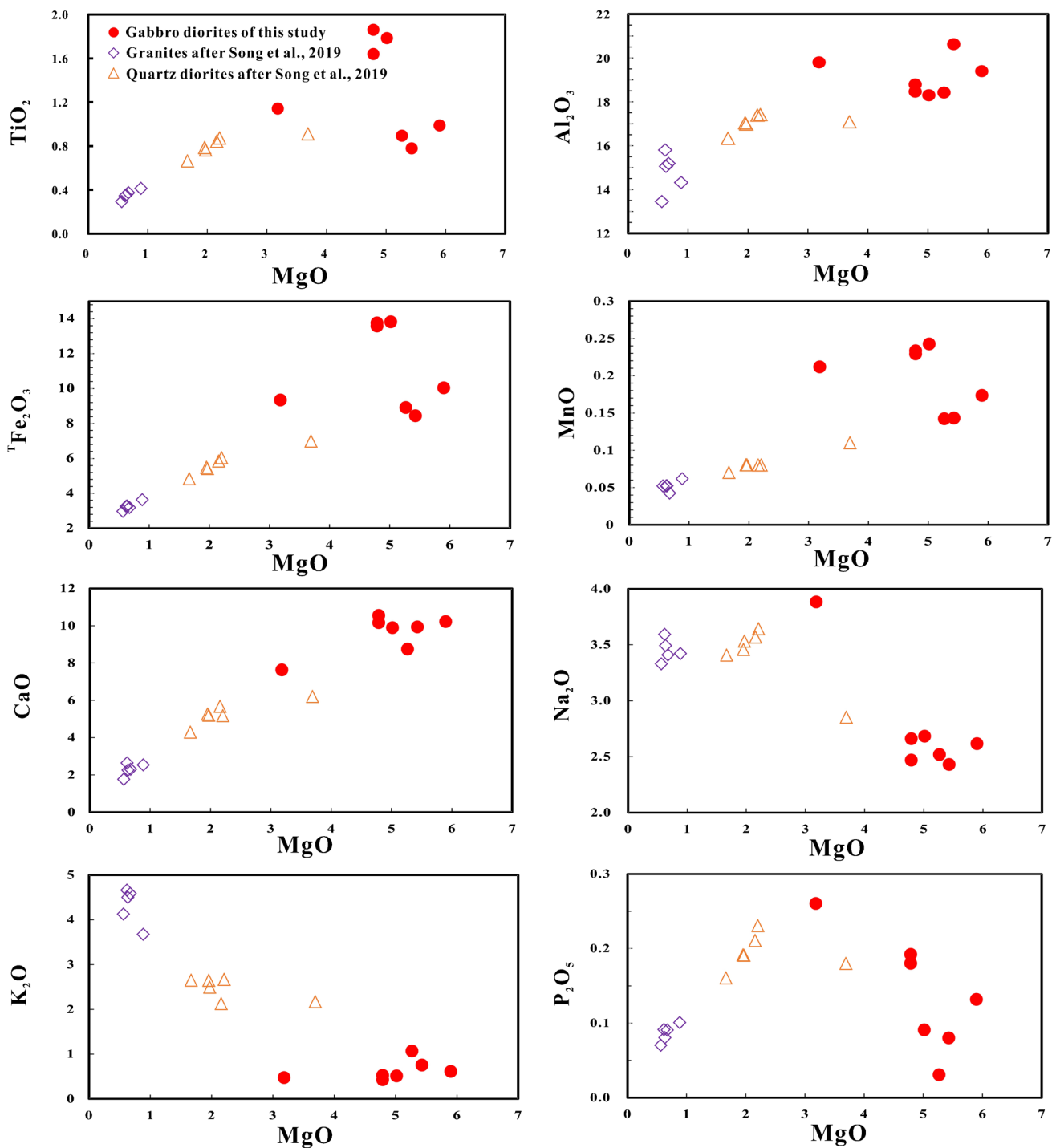


Fig. 8 (a) A/CNK versus A/NK diagram (Maniar and Piccoli 1989). (b)  $K_2O$  versus  $SiO_2$  diagram (modified after Rickwood 1989)

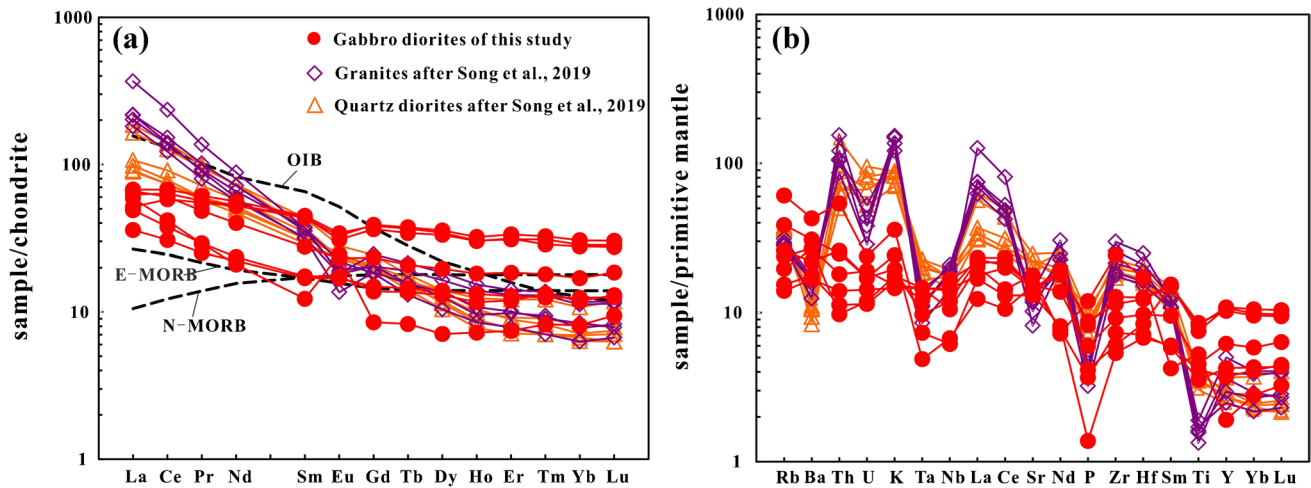


**Fig. 9** Harker diagrams of the Hongshuihe gabbro diorites from the Hongshuihe area in the EKO

REE distribution pattern curves of these two are quite different, indicating that they were formed in different source regions as well. The REE distribution curves of the samples in this study were generally similar to those of island arc magmatic rocks (Wilson 1989; Henderson 1984).

The primitive-mantle-normalized variation spiderweb map of trace elements showed that LILEs (Rb, Ba, K, and

Th) and LREEs are enriched, while HFSEs (Nb, Ta, and Ti) are depleted and P has a negative anomaly. The slight difference in large ion lithophile elements suggests that these rocks were disturbed by some factor, which may be related to fluid metasomatism. The geochemical characteristics of the trace elements in the rocks are consistent with the magmatic



**Fig. 10** (a) Chondrite-normalized REE patterns of the Hongshuihe gabbro diorites from the Hongshuihe area in the EKO. (b) Primitive mantle-normalized variation spiderweb map of the Hongshuihe gabbro diorites from the Hongshuihe area in the EKO. The normalization

values of chondrite are from Boynton (1984); the normalization values of the primitive mantle, N-MORB, E-MORB, and OIB are from McDonough and Sun (1989)

products in the island arc area of the active continental margin (Pearce et al. 1984; Marjorie 1989).

In conclusion, the Hongshuihe rocks in this study were determined to be gabbro diorite, and the samples are intermediate-basic, quasi aluminum, and calc-alkaline series rocks.

### Origin and petrogenesis

Regarding the origin of intermediate-basic magma, there are generally several viewpoints as follows: partial melting of basaltic magma, fluid–melt interactions and fractional crystallization (FC) of mantle-derived primitive magma, or magmatic mixing (Dou et al. 2020; Dong et al. 2018).

The Hongshuihe gabbro diorites are characterized by low  $\text{SiO}_2$  (the mean value is 49.89%) and high  $\text{Mg}^\#$  (the mean value is 47), and they are rich in sodium ( $\text{Na}_2\text{O}/\text{K}_2\text{O} = 2.31 \sim 8.46$ ) and transitional elements. The Nb/Ta ratios of the samples ranged from 12.5 to 24, with an average of 18.58, slightly higher than the Nb/Ta ratios of the mantle (17.5) (Sun and McDonough 1989) and much higher than the Nb/Ta ratios of the continental crust (Taylor and Mclennan 1985). The Zr/Hf ratios of the samples ranged from 26.15 to 51.32, with an average of 35.43, close to the Zr/Hf ratio of mid-ocean ridge basalts (36) (Taylor and Mclennan 1985), indicating that the Hongshuihe gabbro diorites' magma source area should be the mantle source region. In general, rocks derived from asthenosphere mantle basalt have the characteristics of a La/Nb ratio  $< 1.5$  and a La/Ta ratio  $< 22$ . The average La/Nb ratio of the samples was 1.73, while that of the gabbro diorites in this study was greater than 22 (except for the sample 18HSH02-B1, which had a

ratio of 20.33), with an average of 31.44, which means that the rocks derived from the lithospheric mantle rather than the asthenosphere mantle. Moreover, the Rb/Sr ratio of the samples ranged from 0.029 to 0.14 with an average value of 0.06, which is far smaller than that of the crust (0.35) and close to that of the upper mantle (0.034) (Taylor and Mclennan 1995). The Rb/Ba ratios ranged from 0.08 to 0.13 with an average value of 0.09, which is similar to the Rb/Ba ratio of the upper mantle (0.088) (Sun and McDonough 1989). Therefore, the magma source region of Hongshuihe gabbro diorites was the upper mantle.

Rare earth elements are usually less affected by mantle depletion or fluid metasomatism, so they are often used to reflect the characteristics of the parent magma in the magma source area. The samples'  $(\text{Tb}/\text{Yb})_N$  ratio was low (1.03 ~ 1.29; the average value was 1.19), indicating that the rocks were mainly derived from the partial melting of the spinel lherzolite (Wang et al. 2002). According to the discrimination diagram of Sm-Sm/Yb (Fig. 12a), the overall melting trend of the samples of the Hongshuihe gabbro diorites is consistent with the partial melting trend curve of spinel lherzolite, indicating that the rocks are the products of partial melting of spinel lherzolite (about 5 ~ 30%). In addition, the samples have a low Ce/Y ratio (0.72 ~ 2.93, with an average of 1.28), and the samples are mainly located in the stable region of spinel on the  $(\text{La}/\text{Sm})_N - (\text{Tb}/\text{Yb})_N$  diagram (Fig. 12b), suggesting that the rocks were from the relative stable region of spinel (a depth of about 60 km).

The trace elements of the rock show the characteristics of depletion in HFSEs (Ta, Ti) and enrichment in LILEs (Rb, Ba, K), indicating that the magma source area may be contaminated with crustal materials. The Ce/Pb ratio of

**Table 2** Major (wt%) and trace elements (ppm) in the Hongshuihe gabbro diorites from the Hongshuihe area in the EKO

	HSH03-B1	HSH04-B1	HSH05-B1	18HSH01-B1	18HSH02-B1	18HSH03-B1	18HSH04-B1
SiO <sub>2</sub>	47.44	54.01	53.74	50.74	47.37	49.41	46.52
TiO <sub>2</sub>	1.63	1.14	0.89	0.77	1.78	0.98	1.85
Al <sub>2</sub> O <sub>3</sub>	18.36	19.78	18.33	20.40	18.24	19.24	18.68
<sup>T</sup> Fe <sub>2</sub> O <sub>3</sub>	13.66	9.30	8.91	8.39	13.84	10.00	13.56
MnO	0.23	0.21	0.14	0.14	0.24	0.17	0.23
MgO	4.76	3.18	5.24	5.37	5.00	5.85	4.76
CaO	10.16	7.58	8.67	9.78	9.82	10.10	10.45
Na <sub>2</sub> O	2.64	3.89	2.50	2.41	2.67	2.60	2.45
K <sub>2</sub> O	0.44	0.46	1.08	0.73	0.53	0.59	0.49
P <sub>2</sub> O <sub>5</sub>	0.18	0.26	0.03	0.08	0.09	0.13	0.19
LOI	0.70	0.18	1.01	1.22	0.80	0.79	0.67
Total	100.13	100.09	100.51	100.12	100.50	99.98	100.09
σ	2.14	1.72	1.19	1.27	2.34	1.59	2.46
A/CNK	0.79	0.96	0.87	0.90	0.80	0.83	0.79
A/NK	3.81	2.87	3.47	4.29	3.67	3.91	4.10
Mg <sup>#</sup>	0.41	0.40	0.54	0.56	0.42	0.54	0.41
Li	10.90	10.90	20.10	15.60	9.70	11.80	6.30
Be	0.75	0.97	0.64	0.61	0.76	0.71	0.69
Sc	41.70	10.00	20.70	19.20	44.50	27.20	44.80
V	249.00	68.00	179.00	162.00	385.00	204.00	327.00
Cr	13.00	12.00	19.00	24.00	11.00	27.00	13.00
Co	28.70	16.10	27.70	28.00	28.70	31.00	27.60
Ni	2.10	4.10	9.00	11.20	1.50	6.50	1.10
Cu	15.20	7.40	3.50	3.90	8.20	13.00	13.00
Ga	22.20	20.80	17.30	18.00	22.30	19.90	22.40
Rb	8.90	15.10	38.70	24.50	12.50	16.50	9.80
Ba	117.00	188.50	299.00	216.00	186.50	154.00	124.00
Sr	303.00	376.00	277.00	320.00	306.00	322.00	311.00
Y	48.90	8.70	16.90	19.30	49.40	28.10	46.80
Zr	143.00	272.00	60.00	82.00	68.00	103.00	128.00
Nb	10.00	7.50	4.40	4.80	10.30	8.50	11.90
Sn	1.00	1.00	1.00	1.20	1.30	0.80	1.20
Cs	0.66	1.26	2.39	1.42	0.82	1.30	0.88
La	16.00	14.00	11.60	8.50	12.20	15.60	14.80
Ce	41.30	25.50	23.10	18.80	35.50	36.90	38.90
Pr	5.82	2.75	2.77	2.39	5.23	4.60	5.38
Nd	26.20	9.80	11.00	10.40	24.40	18.70	24.80
Sm	6.85	1.88	2.67	2.60	6.64	4.23	6.71
Eu	1.98	1.42	1.01	0.98	1.90	1.34	1.79
Gd	7.86	1.75	2.83	3.06	7.99	4.80	7.47
Tb	1.37	0.31	0.51	0.54	1.40	0.78	1.28
Dy	8.72	1.80	3.31	3.55	9.06	4.99	8.45
Ho	1.72	0.41	0.66	0.75	1.82	1.03	1.71
Er	5.13	1.23	1.98	2.12	5.54	3.06	5.20
Tm	0.79	0.21	0.34	0.32	0.83	0.46	0.73
Yb	4.86	1.38	2.02	2.12	5.20	2.88	4.72
Lu	0.72	0.24	0.33	0.32	0.77	0.47	0.70
Hf	3.90	5.30	2.10	2.20	2.60	3.00	3.80
Ta	0.60	0.60	0.30	0.20	0.60	0.40	0.50
Pb	5.50	6.30	4.70	5.40	4.20	4.70	4.40

**Table 2** (continued)

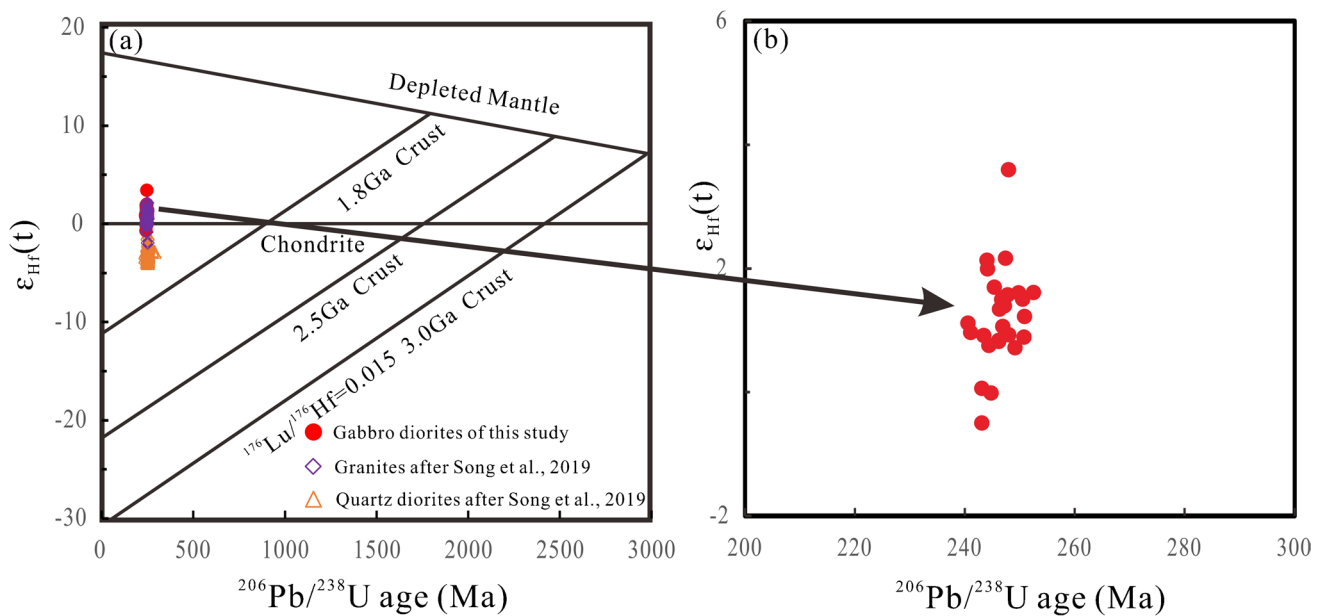
	HSH03-B1	HSH04-B1	HSH05-B1	18HSH01-B1	18HSH02-B1	18HSH03-B1	18HSH04-B1
Th	1.19	1.54	4.57	2.11	0.83	2.21	0.96
U	0.30	0.40	0.50	0.36	0.25	0.36	0.24
ΣREE	129.32	62.68	64.13	56.45	118.48	99.84	122.64
LREE	98.15	55.35	52.15	43.67	85.87	81.37	92.38
HREE	31.17	7.33	11.98	12.78	32.61	18.47	30.26
LREE/HREE	3.15	7.55	4.35	3.42	2.63	4.41	3.05
(La/Yb) <sub>N</sub>	2.36	7.28	4.12	2.88	1.68	3.89	2.25
(La/Sm) <sub>N</sub>	1.47	4.68	2.73	2.06	1.16	2.32	1.39
δEu	0.82	2.35	1.12	1.06	0.80	0.91	0.77

**Table 3** LA-ICP-MS in situ analysis of the zircon Lu–Hf isotopic composition for the Hongshuihe gabbro diorites from the Hongshuihe area in the EKO

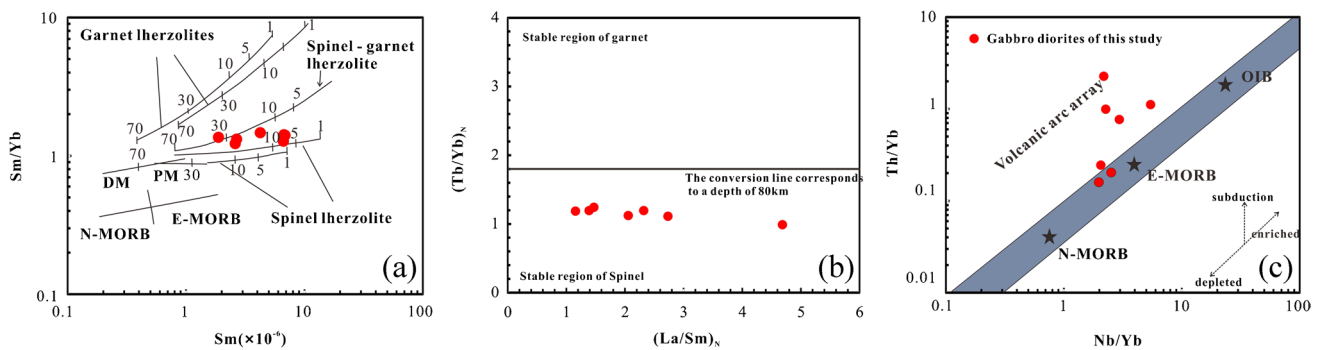
Spot	t (Ma)	<sup>176</sup> Yb/ <sup>177</sup> Hf	2σ	<sup>176</sup> Lu/ <sup>177</sup> Hf	2σ	<sup>176</sup> Hf/ <sup>177</sup> Hf	2σ	ε <sub>Hf</sub> (0)	ε <sub>Hf</sub> (t)	2σ	T <sub>DM1</sub>	T <sub>DM2</sub>	fLu/Hf
HSH05-B1													
01	248	0.019436	0.000264	0.000936	0.000014	0.282648	0.000018	-4.4	0.9	0.6	853	1215	-0.97
02	247	0.006101	0.000085	0.000287	0.000004	0.282650	0.000016	-4.3	1.1	0.6	837	1206	-0.99
03	244	0.010484	0.000046	0.000526	0.000002	0.282644	0.000017	-4.5	0.8	0.6	850	1224	-0.98
04	243	0.021403	0.000912	0.001036	0.000041	0.282627	0.000018	-5.1	0.1	0.6	885	1267	-0.97
05	245	0.013809	0.000073	0.000655	0.000002	0.282623	0.000018	-5.3	0.0	0.7	883	1273	-0.98
06	244	0.023205	0.000346	0.001098	0.000016	0.282682	0.000016	-3.2	2.0	0.6	810	1145	-0.97
07	241	0.018352	0.000172	0.000839	0.000007	0.282658	0.000015	-4.0	1.1	0.5	838	1198	-0.97
08	243	0.016320	0.000086	0.000736	0.000004	0.282610	0.000017	-5.7	-0.5	0.6	902	1302	-0.98
09	244	0.016982	0.000279	0.000792	0.000009	0.282684	0.000016	-3.1	2.1	0.6	800	1136	-0.98
10	251	0.008645	0.000019	0.000410	0.000001	0.282661	0.000017	-3.9	1.5	0.6	824	1181	-0.99
11	243	0.036633	0.001312	0.001705	0.000055	0.282654	0.000022	-4.2	0.9	0.8	862	1213	-0.95
12	241	0.015045	0.000085	0.000750	0.000004	0.282653	0.000019	-4.2	1.0	0.7	843	1208	-0.98
13	248	0.010504	0.000200	0.000496	0.000010	0.282665	0.000015	-3.8	1.6	0.5	821	1174	-0.99
14	247	0.024014	0.000270	0.001102	0.000013	0.282685	0.000016	-3.1	2.2	0.6	806	1136	-0.97
15	245	0.018021	0.000543	0.000818	0.000023	0.282671	0.000018	-3.6	1.7	0.6	819	1165	-0.98
16	247	0.016684	0.000098	0.000776	0.000003	0.282665	0.000018	-3.8	1.5	0.6	827	1178	-0.98
17	251	0.009977	0.000143	0.000468	0.000007	0.282653	0.000016	-4.2	1.2	0.6	837	1199	-0.99
18	246	0.011153	0.000131	0.000497	0.000006	0.282645	0.000014	-4.5	0.8	0.5	849	1221	-0.99
19	252	0.015040	0.000212	0.000706	0.000009	0.282664	0.000015	-3.8	1.6	0.5	826	1176	-0.98
20	247	0.017849	0.000052	0.000787	0.000003	0.282661	0.000015	-3.9	1.4	0.5	832	1185	-0.98
21	249	0.011368	0.000069	0.000533	0.000003	0.282640	0.000016	-4.7	0.7	0.6	856	1229	-0.98
22	251	0.011161	0.000032	0.000515	0.000001	0.282644	0.000015	-4.5	0.9	0.5	850	1220	-0.98
23	248	0.015166	0.000179	0.000704	0.000007	0.282723	0.000015	-1.7	3.6	0.5	744	1045	-0.98
24	246	0.010519	0.000056	0.000497	0.000003	0.282659	0.000016	-4.0	1.3	0.6	829	1188	-0.99
25	246	0.015385	0.000291	0.000688	0.000012	0.282646	0.000020	-4.5	0.8	0.7	851	1220	-0.98
26	250	0.010273	0.000117	0.000473	0.000004	0.282664	0.000019	-3.8	1.6	0.7	821	1174	-0.99

the typical mantle is 25, and the Ce/Pb ratio of the crust is relatively small (< 4.1) (Hofmann 1988). The Ce/Pb ratio of the samples of the Hongshuihe gabbro diorites is 3.48 ~ 8.84, with an average value of 6.44, indicating that some crust-derived materials may have been added into the rock source area. However, the ratios of Nb/Ta and Zr/Hf

are, respectively, 18.58 and 35.43, which are similar to those of original mantle values (Nb/Ta = 17.5, Zr/Hf = 36.27) and higher than the continental crust average values (Nb/Ta = 11, Zr/Hf = 33) (Taylor and Mclennan 1985; Stolz et al. 1996). This implies that the rock mass may not have been obviously contaminated by the crustal region or else were only



**Fig. 11** (a) Diagram of  $^{206}\text{Pb}/^{238}\text{U}$  ages vs. the  $\epsilon_{\text{Hf}}(t)$  of HSH05-B1 zircons in the Hongshuihe gabbro diorites. (b) Partially enlarged view of (a)



**Fig. 12** Discrimination diagram of the Wang et al. 2002 source area of the Hongshuihe gabbro diorites from the Hongshuihe area in the EKO: (a) modified after Zhao and Zhou 2007; (b) modified after; (c) modified after Pearce 2008

weakly contaminated. In general, high La/Sm values ( $> 4.5$ ) indicate contamination by crustal materials (Lassiter and Depaolo 1997). The La/Sm of the Hongshuihe gabbro diorites samples was 1.84~7.45, with a wide range of variation. Except for the sample HSH04-B1 (7.45), the La/Sm ratio of most samples was less than 4.5, indicating that the degree of contamination by continental crust material during the diagenetic process was small and uneven.

Previous studies have suggested that if the  $^{176}\text{Hf}/^{177}\text{Hf}$  value is high ( $\geq 0.282722$ ), the corresponding  $\epsilon_{\text{Hf}}(t)$  value is positive or zero, indicating that the magma source area is depleted mantle or new crust. However, zircons from the old crust or enriched mantle have low  $^{176}\text{Hf}/^{177}\text{Hf}$  values, and the  $\epsilon_{\text{Hf}}(t)$  values of the old crust are usually negative, while the  $\epsilon_{\text{Hf}}(t)$  value of the enriched mantle may be a small positive or negative value (Yang et al. 2018; Wu et al. 2007;

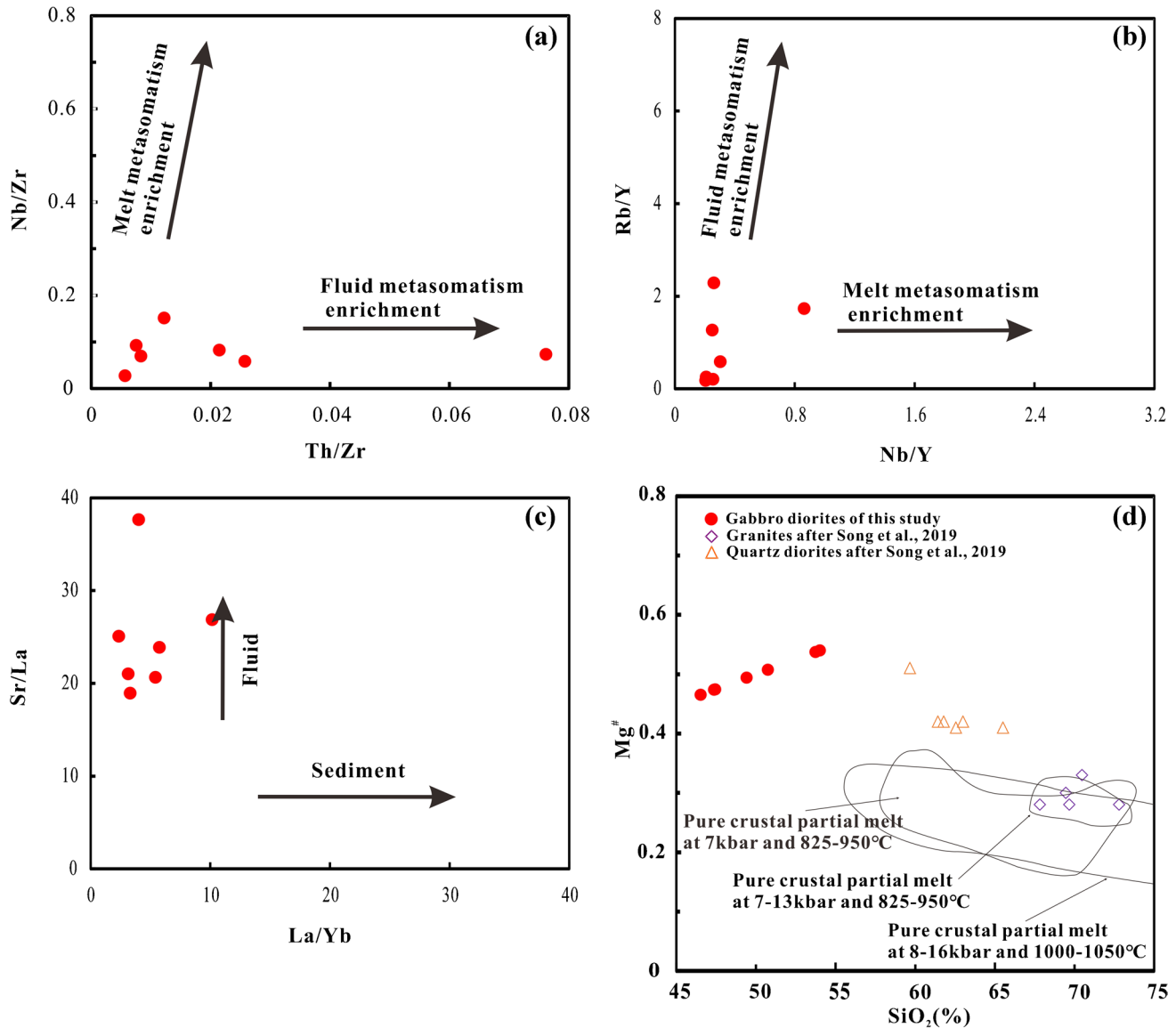
Diwu et al. 2012). The zircon  $^{176}\text{Hf}/^{177}\text{Hf}$  value of the samples ranged from 0.282610 to 0.282685, and the  $\epsilon_{\text{Hf}}(t)$  value ranged from  $-0.5$  to 3.6 (with a mean of 1.27, which is a small positive value), indicating that the rocks were derived from enriched mantle.

The Nb/Th ratios of the samples ranged from 0.96 to 12.41, and were basically less than 10, which did not conform with the characteristics of the OIB mantle, which has a high Nb/Th ratio ( $> 10$ ) (Jochum et al. 1991). This suggests that the samples were unlikely to have derived from the OIB mantle. The Th/Yb–Nb/Yb diagram (Fig. 12c) shows that most of the samples are located above the enriched mantle sequence, indicating that the mantle source area was metasomatically enriched by subduction components (Pearce and Peate 1995). Generally, the mantle source area is contaminated by crustal materials through metasomatism



of subduction slabs, sediment melts, or subduction fluids. Partial melting of subducted slabs usually forms adakite magma. The  $(La/Yb)_N$  of the samples ranged from 1.68 to 7.28, and the LREEs of the Hongshuihe gabbro diorite samples were slightly enriched compared with the HREEs. It is inconsistent with the characteristics of adakite rocks which have strong LREE differentiation model (Defant and Kepezhinskas 2001; Tang and Wang 2010). The ratios of trace elements (Th/Nb, Ba/Th) can effectively identify the effects of sediments and water-bearing fluids in the subduction zone. The Hongshuihe gabbro diorite samples have

relatively stable Th/Nb ratios (0.12~1.04) and a wide range of Ba/Th ratios (65.43~224.7), indicating that water-bearing fluid entered the mantle source area (Tian et al. 2011; Hanyu et al. 2006; Woodhead et al. 2001). The low Zr/Y values (except for that of the sample HSH04-B1, which is 31.26; the others are all less than 4) also reflect the characteristics of the source area of the fluid metasomatism mantle wedge (Gill 1981). The discriminant diagram of contamination in the source region (Fig. 13a–c) supports this argument as well, indicating that the source region was mainly metasomatic through fluids rather than slab or sediment melts.



**Fig. 13** Discrimination diagram of contamination in the source region of the gabbro diorites from the Hongshuihe area in the EKO: (a, b) modified after Kepezhinskas et al. 1997; (c) modified after He et al. 2016; (d) modified after Song et al. 2019.  $Mg^\#$ , molecular  $MgO/(MgO+Fe_2O_{3T})$ . The fields of pure crustal partial melts were obtained in experimental studies by dehydration melting of low-K

basaltic rocks at 8–16 kbar and 1000–1050°C (Rapp and Watson 1995), moderately hydrous (1.7–2.3 wt%  $H_2O$ ) and medium to high-K basaltic rocks at 7 kbar and 825–950 °C (Sisson et al. 2005), and pelitic rocks at 7–13 kbar and 825–950 °C (Patiño Douce and Johnston 1991)

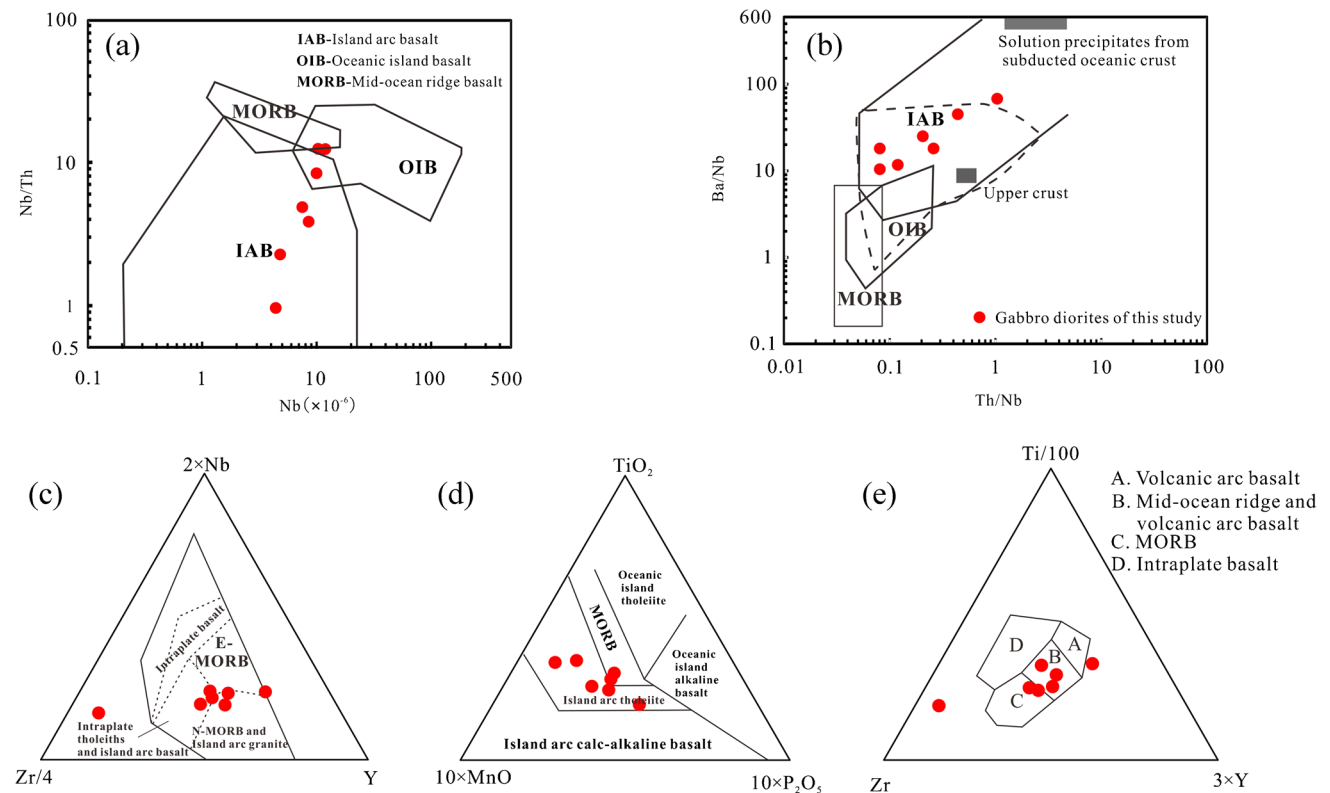
In conclusion, the Hongshuihe gabbro diorites were derived from partially melted spinel lherzolite in the enriched mantle and were weakly contaminated by the crust.

Compared with the Hongshuihe gabbro diorites of this study, previous studies have suggested that the origin of the Hongshuihe quartz diorites and granites could be thickened lower crust, while the quartz diorites have their source in the lower parts of the lower crust, and granites are from the upper parts (Song et al. 2019). In the diagram of  $\text{SiO}_2\text{-Mg}^\#$  (Fig. 13b), most of the Hongshuihe granites samples fell within the pure crustal partial melt region, with another two falling outside the zone, suggesting that the quartz diorites could be mixed with mantle magma. To sum up, the three rocks could be a series of rocks produced by the mantle magma intruding into the lower crust.

### Tectonic significance and implications of the Triassic tectonic evolution of the EKO

The Th/Ta ratios of the Hongshuihe gabbro diorites were 1.38 ~ 15.23, with an average value of 5.59 ( $> 3$ ). Previous studies have shown that the Th/Ta ratio of rocks formed in the island arc environment is generally greater than 3. The

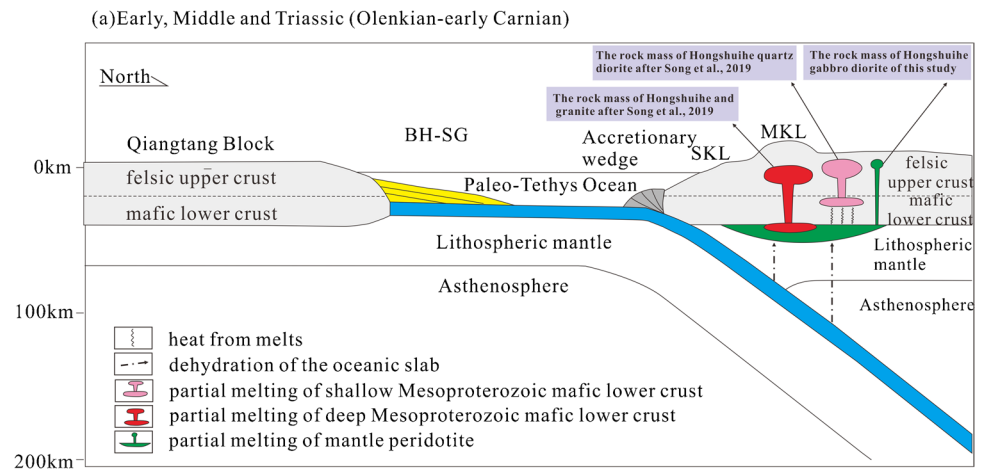
Th/Ta ratio obtained from the samples obviously aligns with this characteristic. The Nb/La ratios of the samples were 0.38 ~ 0.84, which were all less than 1, and the Hf/Ta ratios were 4.33 ~ 11 (except for the sample 18HSH02-B1), which were all significantly greater than 5. The La/Ta ratios were 20.3 ~ 42.5 ( $> 15$ ), the content of Nb was  $4.4 \times 10^{-6} \sim 11.9 \times 10^{-6}$  ( $< 12 \times 10^{-6}$ ), and the content of Ta was  $0.2 \times 10^{-6} \sim 0.6 \times 10^{-6}$  ( $< 0.7 \times 10^{-6}$ ). These characteristics are obviously different from those of intraplate basalt. The Th/Yb ratios were 0.16 ~ 2.26 ( $> 0.1$ ), the average Nb/La was 0.61 ( $< 0.8$ ), and the Hf/Th ratios were 0.46 ~ 3.96 ( $< 8$ ), which also show the tectonic environment affinity related to the arc. In the Nb-Nb/Th diagram (Fig. 14a) and the Th/Nb-Ba/Nb diagram (Fig. 14b), the gabbro diorites samples are located in the island arc basalt and its vicinity, far away from the OIB and MORB areas, showing that the source area was obviously different from the OIB and MORB. Meanwhile, the samples mostly fall into the region of arc basalt in the 2Nb-Zr/4-Y diagram, the  $\text{TiO}_2\text{-10MnO-10P}_2\text{O}_5$  diagram, and the Ti/100-Zr-3Y diagram (Fig. 14c-e), far away from the region of plate basalt. All these indicate that the Hongshuihe gabbro diorite may have formed in island arc environment. The average value of Zr/Y was 7.11, the ratios



**Fig. 14** Discrimination diagram of the tectonic environment of the Hongshuihe gabbro diorites from the Hongshuihe area in the EKO. (a) Nb/Th versus Nb ( $\times 10^{-6}$ ) (modified after Li 1993); (b) Ba/Nb versus Th/Nb (modified after Li 1993); (c) 2Nb-Zr/4-Y (modified

after Meschede 1986); (d)  $\text{TiO}_2\text{-10MnO-10P}_2\text{O}_5$  (modified after Mullen 1983); (e) Ti/100-Zr-3Y (modified after Pearce and Cann 1973)

**Fig. 15** Schematic diagram showing the Early–Middle Triassic (Olenekian–Anisian) geodynamic evolution of the EKO (modified and revised after Song et al. 2019). EKO, Eastern Kunlun Orogen; BH-SG, Bayan Har–Songpanganzi Terrane; SKL, South Kunlun Belt; MKL, Middle Kunlun Belt



of most samples were greater than 3, the ratios of Ta/Yb were 0.09–0.43, and the average value was 0.17 ( $> 0.1$ ), showing the characteristics of active continental margin arcs (Condie 1989). Therefore, the Hongshuihe gabbro diorites should have formed in the subduction environment of the active continental margin.

According to the results above, the Hongshuihe gabbro diorites were formed in the partial melting of the upper mantle, with slight crustal contamination. This was caused by the subduction of the Paleo-Tethys Ocean under the EKO, and the fluid metasomatism of the intermediate-basic magma formed by the upper mantle. This then intruded upwards into the crust and mixed with crustal materials to form the gabbro diorites (Fig. 15). The Hongshuihe gabbro diorites studied here were formed in the same area at the same time as the  $244 \pm 2$  Ma (Anisian) quartz diorites and the  $246 \pm 1$  Ma (Olenekian) granites found by Song et al. (2019). It is more reasonable to consider the three kinds of rocks in the same tectonic setting. The previous study concluded that the Hongshuihe quartz diorites and granites were formed in the subduction stage before the collision (Song et al. 2019). Combined with analyses of the origin and petrogenesis, it is likely that in the Middle Triassic, the Paleo-Tethys Ocean subducted northward under the EKO, which caused dehydration of the oceanic slab and partial melting of the asthenosphere mantle, and the magma of the mantle intruded into the lower crust. The lower basaltic crust was partially melted to form the Hongshuihe granites. The partly melting asthenosphere mantle, with assimilation of and contamination by crustal materials, cooled and consolidated to form the rock mass of the Hongshuihe gabbro diorites. At the same time, the mantle magma and the basaltic crustal magma partly mixed with each other to form the rock mass of the Hongshuihe quartz diorites.

In conclusion, these rock masses of the Hongshuihe quartz diorites, granites (Song et al. 2019), and gabbro diorites were formed by magma mixing, partial melting of the basaltic lower crust, and partial melting of the asthenosphere mantle with assimilation of and

contamination by crustal materials, respectively. All these indicate that the Paleo-Tethys Ocean was subducted during the Middle Triassic, which is of great significance for perfecting the details of the tectonic evolution process of the Paleo-Tethys Ocean.

## Conclusions

1. The LA-ICP-MS zircon U–Pb dating results of the gabbro diorites from the Hongshuihe area showed that the weighted average zircon  $^{206}\text{Pb}/^{238}\text{U}$  ages are  $238.8 \pm 2.5$  Ma (MSWD = 0.93) and  $246.3 \pm 1.2$  Ma (MSWD = 0.86), with an average of 242 Ma, indicating that the gabbro diorites belong to the early of the Middle Triassic period.
2. The petrogeochemical characteristics showed that the Hongshuihe gabbro diorites derived from partially melted spinel lherzolite in the enriched mantle, weakly contaminated by the crust.
3. The Hongshuihe gabbro diorites in this study and the Hongshuihe quartz diorites and granites were all formed in the same tectonic background of the Paleo-Tethys Ocean subducting northward under the EKO, which caused dehydration of the oceanic slab and partial melting of the asthenosphere mantle; then, the magma of the mantle intruded into the lower crust.

**Acknowledgements** We are grateful to Dr. Lin Peijun from the Analysis Center in the Shandong Bureau of China Metallurgical Geology Bureau, and Dr. Yang Tao from the State Key Laboratory for Mineral Deposit Research, Department of Earth Sciences, in Nanjing University for their assistance with the lab work of LA-ICP-MS zircon dating and the LA-MC-ICP-MS in situ Hf isotopic analyses. We sincerely thank the Associate Editor and peer reviewers for their thoughtful reviews. We thank English editing services listed at <https://www.mdpi.com/authors/english> for professional English editing during the revision of this manuscript.

**Funding** This research was supported by the National Natural Science Foundation of China (Grant No. 41572056) and the Opening Foundation of the Key Laboratory of Mineral Resources Evaluation in North-east Asia, Ministry of Land and Resources.

## Declarations

**Competing interests** The authors declare no competing interests.

## References

- Andersen T (2002) Correction of common lead in U-Pb analyses that do not report  $^{204}\text{Pb}$ . *Chem Geol* 192:59–79. [https://doi.org/10.1016/S0009-2541\(02\)00195-X](https://doi.org/10.1016/S0009-2541(02)00195-X)
- Bao SL, Ye JL, Hao JX, Wang CY, Wu YA (2010) Investigation on the Hongshuihe iron deposit forming reason and ore searching prospect in Dulan county of Qinghai Province. *J Qinghai Univ (Nat Sci)* 28(2):42–46 (in Chinese with English abstract)
- Bian QT, Li DH, Pospelov I, Yin LM, Li HS, Zhao DS et al (2004) Age, geochemistry and tectonic setting of Buqingshan ophiolites, North Qinghai-Tibet Plateau, China. *J Asian Earth Sci* 23:577–596. <https://doi.org/10.1016/j.jseaes.2003.09.003>
- Boynton WV (1984) Cosmochemistry of the rare earth elements: meteorites studies. In P Henderson (Ed) *Rare earth element geochemistry*. Elsevier, New York, pp 63–114. <https://doi.org/10.1016/B978-0-444-42148-7.50008-3>
- Chen GC, Pei XZ, Li RB, Li ZC, Liu CJ, Chen YX et al (2017) Paleo-Tethyan oceanic crust subduction in the eastern section of the East Kunlun Orogenic Belt: geochronology and petrogenesis of the Qushi'ang granodiorite. *Acta Geol Sin (Engl Ed)* 91:565–580. <https://doi.org/10.1111/1755-6724.13118>
- Condie KC (1989) Geochemical changes in basaltic and siltstone across the Archaean Proterozoic boundary: identification and significance. *Lithos* 23:1–18. [https://doi.org/10.1016/0024-4937\(89\)90020-0](https://doi.org/10.1016/0024-4937(89)90020-0)
- Cox KG, Bell JD, Pankhurst RJ (1979) *The interpretation of igneous rocks*. George, Allen and Unwin, London, p 450
- Defant MJ, Kepezhinskas P (2001) Evidence suggests slab melting in arc magmas. *EOS Trans Am Geophys Union* 82(6):65–65. <https://doi.org/10.1029/01EO00038>
- Deng JF, Luo ZH, Su SG, Mo XX, Lai XY, Kan HW (2004) Petrogenesis, tectonic setting and metallogenesis. *Geological Publishing House, Beijing*, pp 1–381. (in Chinese with English abstract)
- Ding QF, Jiang SY, Sun FY (2014) Zircon U-Pb geochronology, geochemical and Sr-Nd-Hf isotopic compositions of the Triassic granite and diorite dikes from the Wulonggou mining area in the Eastern Kunlun Orogen, NW China: petrogenesis and tectonic implications. *Lithos* 205:266–283. <https://doi.org/10.1016/j.lithos.2014.07.015>
- Ding QF, Liu F, Yan W (2015) Zircon U-Pb geochronology and Hf isotopic constraints on the petrogenesis of Early Triassic granites in the Wulonggou area of the Eastern Kunlun Orogen, Northwest China. *Int Geol Rev* 57:1–20. <https://doi.org/10.1080/00206814.2015.1029541>
- Diwu CR, Sun Y, Wang Q (2012) The crustal growth and evolution of North China Craton: revealed by Hf isotopes in detrital zircons from modern rivers. *Acta Petrol Sin* 28(11):3520–3530. [https://doi.org/10.1007/978-981-10-1064-4\\_2](https://doi.org/10.1007/978-981-10-1064-4_2)
- Dong CY, Wang C, Xie HQ, Bai WQ, Wan YS (2018) Late Neoproterozoic Jielingkou diorite in eastern Hebei, North China Craton: origin from U-Pb-Nd-Hf-O isotopic studies. *Acta Petrol Sin* 34(9):2793–2810 (in Chinese with English abstract)
- Dou XF, Chen X, Zheng YY, Jiang XJ, Wang JS, Zheng SL, Ren H, Yang C, Zhu JH (2020) The newly discovered Cambrian gabbrodiorite in Bange, Tibet: Tectonic Implications. *Earth Sci* 45(6):2091–2102 (in Chinese with English abstract)
- Gill JB (1981) *Orogenic andesites and plate tectonics*. Springer Verlag, New York, p 385. <https://doi.org/10.1007/978-3-642-68012-0>
- Gou J, Sun DY, Ren YS et al (2013) Petrogenesis and geodynamic setting of Neoproterozoic and Late Paleozoic magmatism in the Manzhouli-Erguna area of Inner Mongolia, China: geochronological, geochemical and Hf isotopic evidence. *J Asian Earth Sci* 67–68:114–137. <https://doi.org/10.1016/j.jseaes.2013.02.016>
- Guan L (2013) Mineralization characteristics of the Hongshui river iron deposit, Dulan county, Qinghai province. Master Dissertation. China University of Geosciences (Beijing) 1–43
- Hanyu T, Tatsumi Y, Nakai S et al (2006) Contribution of slab melting and slab dehydration to magmatism in the NE Japan arc for the last 25 Myr: constraints from geochemistry. *Geochim Geophys Res* 11:1–29. <https://doi.org/10.1029/2005GC001220>
- He HY, Wang YJ, Liu HC, Zhang YZ (2016) Geochemical and geochronological characteristics of the Fengmu mafic rocks in Hainan and its tectonic implications. *J Sun Yat-sen Univ (Nat Sci)* 55(4):146–157 (in Chinese with English abstract)
- Henderson P (1984) *Rare earth element geochemistry*. Elsevier Science Publishers, Amsterdam, pp 33–54. [https://doi.org/10.1016/0012-8252\(85\)90064-9](https://doi.org/10.1016/0012-8252(85)90064-9)
- Hofmann AW (1988) Chemical differentiation of the Earth: the relationship between mantle, continental crust, and oceanic crust. *Earth Planet Sci Lett* 90(3):297–314. [https://doi.org/10.1016/0012-821X\(88\)90132-X](https://doi.org/10.1016/0012-821X(88)90132-X)
- Hou KJ, Li YH, Zou TR, Qu XM, Shi YR, Xie GQ (2007) Laser ablation-MC-ICP-MS technique for Hf isotope microanalysis of zircon and its geological applications. *Acta Petrol Sin* 23:2595–2604
- Jiang CF, Yang JS, Feng BG, Zhu ZX, Zhao M, Chai YC, Wang HD (1992) Opening closing tectonics of Kunlun Shan. *Geological Memoirs, Series 5*. Beijing: Geological Publishing House, pp 1–217. Number 12. (in Chinese with English abstract)
- Jochum KP, Arndt NT, Hofmann AW (1991) Nb-Th-La in komatiites and basalts: constraints on komatiite petrogenesis and mantle evolution. *Earth Planet Sci Lett* 107(2):272–289. [https://doi.org/10.1016/0012-821X\(91\)90076-T](https://doi.org/10.1016/0012-821X(91)90076-T)
- Kepezhinskas P, McDermott F, Defant MJ et al (1997) Trace element and Sr-Nd-Pb isotopic constraints on a three-component model of Kamchatka Arc petrogenesis. *Geochim Cosmochim Acta* 61(3):577–600. [https://doi.org/10.1016/S0016-7037\(96\)00349-3](https://doi.org/10.1016/S0016-7037(96)00349-3)
- Lassiter JC, Depaolo DJ (1997) Plume-lithosphere interaction in the generation of continental and oceanic flood basalts: chemical and isotopic constraints. *Am Geophys Union (AGU)* 100:335–355
- Le Bas MJ, LeMaitre RW, Streckeisen AL, Zanettin B (1986) A chemical classification of volcanic rocks based on the total alkali-silica diagram. *J Petrol* 27:745–750. <https://doi.org/10.1093/petrology/27.3.745>
- Li CD, Zhang FQ, Miao LC, Xie HQ, Xu YW (2007) Zircon SHRIMP geochronology and geochemistry of Late Permian high-Mg andesites in Shehuohe area, Jilin province, China. *Acta Petrol Sin* 23(4):767–776 (in Chinese with English abstract)
- Li SG (1993) Ba-Th-Nb-La discriminant diagram of the tectonic setting of ophiolite formation. *Acta Petrol Sin* 9(2):146–157 (in Chinese with English abstract)
- Liu B, Ma CQ, Zhang JY, Xiong FH, Huang J, Jiang HA (2012) Petrogenesis of Early Devonian intrusive rocks in the east part of Eastern Kunlun Orogen and implication for Early Palaeozoic orogenic processes. *Acta Petrol Sin* 28(6):1785–1807 (in Chinese with English abstract)

- Liu SB, Zhang AK, Liu GL, Zhou QL, Zhang DM, Wang SM (2016) Geological characteristics of the Hongshuihe iron-manganese deposit in Eastern Kunlun Metallogenic Belt and its discovery significance. *Northwest Geol* 49(01):197–205 (in Chinese with English abstract)
- Liu YJ, Genser J, Neubauer F, Jin W, Ge XH, Handler R, Takasu A (2005)  $^{40}\text{Ar}/^{39}\text{Ar}$  mineral ages from basement rocks in the Eastern Kunlun Mountains, NW China, and their tectonic implications. *Tectonophysics* 398:199–224. <https://doi.org/10.1016/j.tecto.2005.02.007>
- Liu YS, Hu ZC, Gao S, Günther D, Xu J, Gao CG, Chen HH (2008) In situ analysis of major and trace elements of anhydrous minerals by LA-ICP-MS without applying an internal standard. *Chem Geol* 257:34–43. <https://doi.org/10.1016/j.chemgeo.2008.08.004>
- Liu YS, Hu ZC, Zong KQ, Gao CG, Gao S, Xu J, Chen HH (2010) Reappraisal and refinement of zircon U-Pb isotope and trace element analyses by LA-ICP-MS. *Chin Sci Bull* 55:1535–1546. <https://doi.org/10.1007/s11434-010-3052-4>
- Ludwig KR (2003) ISOPLOT 3.00, a geochronology toolkit for Microsoft Excel. Berkeley: Berkeley Geochronological Center Special Publication
- Maniar PD, Piccoli PM (1989) Tectonic discrimination of granitoids. *Geol Soc Am Bull* 101:635–643. [https://doi.org/10.1130/0016-7606\(1989\)101%3c0635:TDOG%3e2.3.CO;2](https://doi.org/10.1130/0016-7606(1989)101%3c0635:TDOG%3e2.3.CO;2)
- Marjorie W (1989) Igneous petrogenesis. Unwin Hyman Inc, London, pp 153–226. <https://doi.org/10.1180/minmag.1989.053.372.15>
- Meschede M (1986) A method of discriminating between different types of mid-ocean ridge basalts and continental tholeiites with the Nb-Zr-Y diagram. *Chem Geol* 56(3–4):207–218. [https://doi.org/10.1016/0009-2541\(86\)90004-5](https://doi.org/10.1016/0009-2541(86)90004-5)
- Mo XX, Luo ZH, Deng JF, Yu XH, Liu CD, Zhan HW, Liu YH (2007) Granitoids and crustal growth in the East-Kunlun Orogenic Belt. *Geol J China Univ* 13(3):403–414 (in Chinese with English abstract)
- Mullen ED (1983) MnO/TiO<sub>2</sub>/P<sub>2</sub>O<sub>5</sub>: a minor element discriminate for basaltic rocks of oceanic environments and its implications for petrogenesis. *Earth Planet Sci Lett* 1(62):53–62. [https://doi.org/10.1016/0012-821X\(83\)90070-5](https://doi.org/10.1016/0012-821X(83)90070-5)
- Patiño Douce AE, Johnston AD (1991) Phase equilibria and melt productivity in the pelitic system: implications for the origin of peraluminous granitoids and aluminous granulites. *Contrib Miner Petrol* 107:202–218. <https://doi.org/10.1007/BF00310707>
- Pearce JA, Cann JR (1973) Tectonic setting of basic volcanic rocks determined using trace element analyses. *Earth Planet Sci Lett* 19(2):290–300. [https://doi.org/10.1016/0012-821X\(73\)90129-5](https://doi.org/10.1016/0012-821X(73)90129-5)
- Pearce JA (2008) Geochemical fingerprinting of oceanic basalts with applications to ophiolite classification and the search for Archean oceanic crust. *Lithos* 100(1–4):14–48. <https://doi.org/10.1016/j.lithos.2007.06.016>
- Pearce JA, Lippard SJ, Robert S (1984) Marginal basin geology : characteristics and tectonic significance of supra-subduction zone ophiolite. *Geol Soc Lond Spec Publ* 16:77–94
- Pearce JA, Peate DW (1995) Tectonic implications of the composition of volcanic arc magmas. *Ann Rev Earth Planet Sci* 23(1):251–285. <https://doi.org/10.1146/annurev.ea.23.050195.001343>
- Rapp RP, Watson EB (1995) Dehydration melting of metabasalt at 8–32 kbar: Implications for continental growth and crust–mantle recycling. *J Petrol* 36(4):891–931. <https://doi.org/10.1093/ptology/36.4.891>
- Rickwood PC (1989) Boundary lines within petrologic diagrams which use oxides of major and minor elements. *Lithos* 22(4):247–263. [https://doi.org/10.1016/0024-4937\(89\)90028-5](https://doi.org/10.1016/0024-4937(89)90028-5)
- Shen YS, Wang CX, Zhang YJ (2009) Study on genesis and geological characteristics of Hongshuihe iron deposit in Qinghai province. *Miner Resour Geol* 23(4):307–310 (in Chinese with English abstract)
- Sisson TW, Ratajeski K, Hankins WB, Glazner AF (2005) Voluminous granitic magmas from common basaltic sources. *Contrib Miner Petrol* 148:635–661. <https://doi.org/10.1007/s00410-004-0632-9>
- Sklyarov EV, Gladkochub DP, Mazukabzov AM (2003) Neoproterozoic mafic dike swarms of the Sharyzhalgai metamorphic massif, southern Siberian craton. *Precamb Res* 122(1):359–376. [https://doi.org/10.1016/S0301-9268\(02\)00219-X](https://doi.org/10.1016/S0301-9268(02)00219-X)
- Song K, Ding QF, Zhang Q et al (2019) Zircon U-Pb geochronology, Hf isotopes, and whole-rock geochemistry of Hongshuihe Early to Middle Triassic quartz diorites and granites in the Eastern Kunlun Orogen, NW China: implication for petrogenesis and geodynamics. *Geol J* 55(2):1507–1528. <https://doi.org/10.1002/gj.3517>
- Stolz AJ, Jochum KP, Spettel B, Hofmann AW (1996) Fluid- and melt-related enrichment in the subarc mantle: evidence from Nb/Ta variations in island-arc basalts. *Geology* 24(7):587–590. [https://doi.org/10.1130/0091-7613\(1996\)0242.3.CO;2](https://doi.org/10.1130/0091-7613(1996)0242.3.CO;2)
- Sun SS, McDonough WF (1989) Chemical and isotopic systematics of oceanic basalts: implications for mantle composition and processes. *Geol Soc Lond Spec Publ* 42(1):313–345. <https://doi.org/10.1144/GSL.SP.1989.042.01.19>
- Tang GJ, Wang Q (2010) High-Mg andesites and their geodynamic implications. *Acta Petrol Sin* 26(8):2495–2512 (in Chinese with English abstract)
- Taylor SR, McLennan S (1995) The geochemical composition of the continental crust. *Rev Geophys* 33:241–265
- Taylor SR, McLennan SM (1985) The continental crust: its composition and evolution. Blackwell Scientific Publications, Oxford, pp 1–328
- Tian LY, Castillo PR, Hilton DR et al (2011) Major and trace element and Sr-Nd isotope signatures of the northern Lau Basin lavas: implications for the composition and dynamics of the Back-arc basin mantle. *J Geophys Res* 116:657–670. <https://doi.org/10.1029/2011JB008791>
- TIGQS (Third Institute of Qinghai Geology Survey) (2014) Geological map of Hongshuihe - Qingshuihe area in Dulan County, Qinghai Province (In Chinese)
- Wang K, Plant T, Walker JD et al (2002) A mantle melting profile across the basin and range, SW USA. *J Geophys Res* 107(B1):ECV 5-1-ECV 5-21. <https://doi.org/10.1029/2001jb000209>
- Wilson M (1989) Igneous Petrogenesis: a global tectonic approach. Unwin Hyman, London, pp 1–466. <https://doi.org/10.1180/minmag.1989.053.372.15>
- Woodhead JD, Hergt JM, Davidson JP, Eggins SM (2001) Hafnium isotope evidence for “conservative” element mobility during subduction zone processes. *Earth Planet Sci Lett* 192(3):331–346. [https://doi.org/10.1016/S0012-821X\(01\)00453-8](https://doi.org/10.1016/S0012-821X(01)00453-8)
- Wu FY, Li XH, Zheng YF, Gao S (2007) Lu-Hf isotopic systematics and their applications in petrology. *Acta Petrol Sin* 23(2):185–220 (in Chinese with English abstract)
- Wu FY, Yang YH, Xie LW, Yang JH, Xu P (2006) Hf isotopic compositions of the standard zircons and baddeleyites used in U-Pb geochronology. *Chem Geol* 234:105–126. <https://doi.org/10.1016/j.chemgeo.2006.05.003>
- Xu ZQ, Yang JS, Li HB, Zhang JX, Wu CL (2007) Terrane amalgamation, collision and uplift in the Qinghai-Tibet Plateau. Geological Publishing House, Beijing (1–458 pp.). (in Chinese with English abstract)
- Yan W, Qiu DM, Ding QF, Liu F (2016) Geochronology, petrogenesis, source and its structural significance of Houtougou monzogranite of Wulonggou area in Eastern Kunlun Orogen. *J Jilin Univ (Earth Sci Ed)* 46(2):443–460 (in Chinese with English abstract)
- Yang JS, Robinson PT, Jiang CF, Xu ZQ (1996) Ophiolites of the Kunlun Mountains, China and their tectonic implications. *Tectonophysics* 258(1–4):215–231. [https://doi.org/10.1016/0040-1951\(95\)00199-9](https://doi.org/10.1016/0040-1951(95)00199-9)

- Yang JS, Xu ZQ, Li HB, Shi RD (2005) The Paleo-Tethyan volcanism and plate tectonic regime in the A'nyemaqen region of East Kunlun, northern Tibet Plateau. *Acta Petrol ET Mineral* 24(5):369–380 (in Chinese with English abstract)
- Yang XM, Sun FY, Zhao TF, Liu JL, Peng B (2018) Zircon U-Pb dating, geochemistry and tectonic implications of Akechukesai gabbro in East Kunlun orogenic belt. *Geol Bull China* 37(10):1842–1852 (in Chinese with English abstract)
- Yuan C, Zhou MF, Sun M, Zhao YJ, Wilder S, Long XP, Yan DP (2010) Triassic granitoids in the eastern Songpan Ganzi Fold Belt, SW China: Magmatic response to geodynamics of the deep lithosphere. *Earth Planet Sci Lett* 290:481–492. <https://doi.org/10.1016/j.epsl.2010.01.005>
- Zhang YM (2017) Indosinian tectonic-magmatism and regional tectonic evolution in the Qinghai-nanshan Tectonic Belt. Doctor Dissertation. Chang'an University, pp 33–57. (in Chinese with English abstract)
- Zhang Q, Zhou GQ (2001) Chinese ophiolite. Science Press, Beijing, pp 1–200
- Zhao JH, Zhou MF (2007) Geochemistry of Neoproterozoic mafic intrusions in the Panzhihua district (Sichuan Province, SW China): implications for subduction-related metasomatism in the upper mantle. *Precamb Res* 152(1–2):27–47 (in Chinese with English abstract)
- Zhang FY, Huo HQ, Hao LH, Fan LK, Cai YP, Dou HW (2009) Analysis on geological characteristics and genesis of Hongshuihe iron ore in Dulan county. *Gold Sci Technol* 17(3):35–39 (in Chinese with English abstract)
- Zhao ZH, Sun DY, Gou J, Ren YS, Fu CL, Zhang XY, Wang X, Liu XM (2011) Chronology and geochemistry of volcanic rocks in Tamulangou Formation from southern Manchuria, Inner-Mongolia. *J Jilin Univ (Earth Sci Ed)* 41(6):1865–1880 (in Chinese with English abstract)